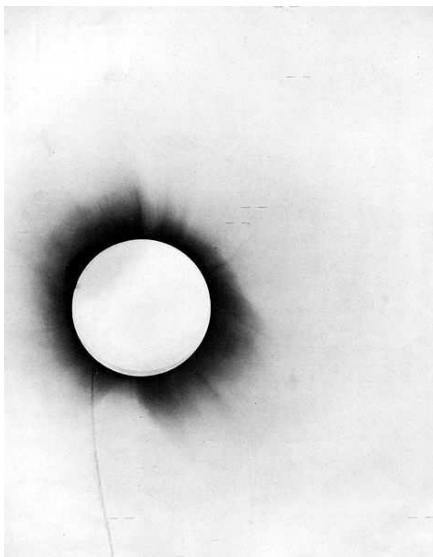


## 1. Introduction

A direct consequence of special relativity is that any sensible theory of gravitation must predict that light bends in the vicinity of a gravity field. As a result, light, or generally any electromagnetic radiation, emitted by a distant object and travelling near a very massive object in the foreground will appear to come from a point away from the real source and produce effects of mirage and of light concentration generally referred to as gravitational lensing.

### 1.1 History

Henry Cavendish in 1784 and Johann Georg von Soldner in 1801 had pointed out that Newtonian gravity might imply that starlight bends around a massive object. In 1911, Soldner's calculation was repeated by Einstein, who noted in 1915, in the process of completing general relativity, that the result is only half the correct value. He became the first to calculate the correct value for light bending [1].



*Figure 1. One of Eddington's photographs of the 1919 solar eclipse experiment, presented in his 1920 paper announcing its success.*

The first observation of light deflection was performed by noting the change in position of stars as they passed near the Sun. In 1919, Sir Arthur Eddington and his collaborators observed a total solar eclipse allowing for such stars to be observed. Observations were made simultaneously in the cities of Sobral and Ceará (Brazil) and São Tomé and Príncipe (west coast of Africa). The result [2] made the front page of most major newspapers and made Einstein and his theory of general relativity world famous. The measurement was repeated by a team from the Lick Observatory in the 1922 eclipse, with results that agreed with the 1919 results and has been repeated several times since, most notably in 1973 by a team from the University of Texas. Considerable uncertainty remained in these measurements for

almost fifty years, until observations started being made at radio frequencies. It was not until the late 1960s that it was definitively shown that the amount of deflection was the full value predicted by general relativity, and not half that number.

The phenomenon of gravitational lensing was first mentioned in 1924 by the St. Petersburg physicist Orest Chwolson [3] and quantified by Einstein in 1936 [4,5]. In his paper, he remarked *“Of course, there is no hope of observing this phenomenon directly. First, we shall scarcely ever approach closely enough to such a central line. Second, the angle  $\beta$  will defy the resolving power of our instruments”*. In this statement, he refers to the need for a perfect alignment to observe rings and his  $\beta$  is the so-called Einstein radius, the angular aperture of the ring. Here, Einstein was only considering the chance of observing rings produced by stars, which is low; however, the chance of observing those produced by larger lenses such as galaxies or black holes is higher since the angular size of an Einstein ring increases with the mass of the lens.

Fritz Zwicky noted in 1937 that the effect could allow galaxy clusters to act as gravitational lenses. It was not until 1979 that this effect was confirmed by observation of the so-called “Twin QSO” SBS 0957+561 (QSO stands for Quasi Stellar Object, more commonly referred to as quasar; the Twin QSO had been discovered accidentally by D. Walsh, B. Carswell and R. Weymann using the Kitt Peak National Observatory 2.1 m telescope) by Roger Lynds of the National Optical Astronomy Observatories and Vahe Petrosian of Stanford University who discovered giant luminous arcs in a survey of galaxy clusters. They published their findings in 1986 without knowing the origin of the arcs. In 1987, Genevieve Soucail of the Toulouse Observatory and her collaborators presented data of a blue ring-like structure in Abell 370 and proposed a gravitational lensing interpretation. J. Anthony Tyson of Bell Laboratories and collaborators conducted the first cluster weak lensing analysis in 1990. Tyson et al. detected a coherent alignment of the ellipticities of the faint blue galaxies behind both Abell 1689 and CL 1409+52 (Abell 1689, a galaxy cluster in the constellation Virgo, is one of the biggest and most massive galaxy clusters known and acts as a gravitational lens, distorting the images of galaxies that lie behind it). In 2006, David Wittman of the University of California at Davis and collaborators published the first sample of galaxy clusters detected via their lensing signals, independently of previous knowledge about them.

In the 1980s, astronomers realized that the combination of CCD imagers and computers would allow the brightness of millions of stars to be measured each night. In a dense field, such as the galactic centre or the Magellanic Clouds, many microlensing events per year could potentially be found. This led to efforts such as the Optical Gravitational Lensing Experiment, or OGLE, which has characterized hundreds of such events.

### 1.2. General features

One commonly distinguishes between three types of gravitational lensing: strong, weak and micro.

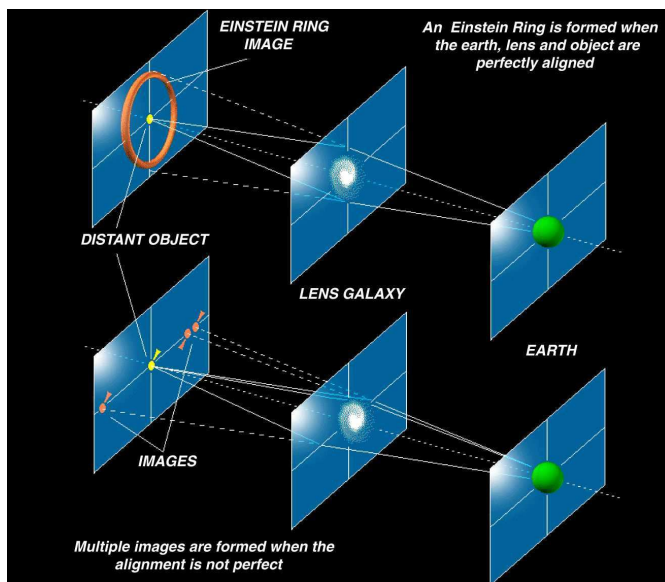


Figure 2. Einstein rings in the case of perfect (top) and approximate (bottom) alignment of the source and of the lens on the line of sight of the observer.

One talks of strong lensing when there are easily visible distortions such as the formation of Einstein rings, arcs, and multiple images. In such cases, the source and the lens are well defined. Ideally, an Einstein ring occurs when the lens and the source are both spherical and exactly on the line of sight of the observer (Figure 2). When the lens or the source is not spherical or when the alignment is not perfect, one observes multiple images of the same source or partial arcs scattered around the lens. The

number and shape of these depends upon the relative positions of the source, lens, and observer, and the shape of the gravitational well of the lensing object.

One talks of weak lensing when the distortions of the background sources are too small, say only a few percent, to allow for an analysis in terms of single source-lens pairs but sufficiently numerous to allow for a statistical analysis. What is then observed is a preferred stretching of the background objects perpendicular to the direction to the centre of the lens. By measuring the shapes and orientations of large

numbers of distant galaxies, their orientations can be averaged to measure the shear of the lensing field in any region. This, in turn, can be used to reconstruct the mass distribution in the area: in particular, the background distribution of dark matter can be reconstructed. Since galaxies are intrinsically elliptical and the weak gravitational lensing signal is small, a very large number of galaxies must be used in these surveys. These weak lensing surveys must carefully avoid a number of important sources of systematic error: the intrinsic shape of galaxies, the tendency of a camera's point spread function to distort the shape of a galaxy and the tendency of atmospheric seeing to distort images must be understood and carefully accounted for.

Finally, microlensing refers to cases where the effect is too small to produce visible distortions in shape, but the amount of light received from a background source is observed to change with time while the source passes behind the lens. Microlensing has been used to search for brown dwarfs in order to evaluate their contribution to dark matter and, more recently, to search for exoplanets with much success.

The lensing object may be stars in the Milky Way in one typical case, with the background source being stars in a remote galaxy, or, in another case, an even more distant quasar. The effect is small, such that (in the case of strong lensing) even a galaxy with a mass more than 100 billion times that of the sun will produce multiple images separated by only a few arc seconds. Galaxy clusters can produce separations of several arc minutes. In both cases the galaxies and sources are quite distant, many hundreds of megaparsecs away from our Galaxy.

Gravitational lenses act equally on all kinds of electromagnetic radiation, not just visible light. Weak lensing effects are being studied for the cosmic microwave background as well as galaxy surveys. Strong lenses have been observed in radio and X-ray regimes as well. If a strong lens produces multiple images, there will be a relative time delay between two paths: that is, in one image the lensed object will be observed before the other image.

Gravitational lenses can be used to study the background source or the foreground lens.

In the first case, they act as gravitational telescopes, because they concentrate the light from objects seen behind them, making very faint objects appear brighter,

larger and therefore more easily studied. Researchers at Caltech have used the strong gravitational lensing afforded by the Abell 2218 cluster of galaxies to detect the most distant galaxy known at the time (February 15, 2004) through imaging with the Hubble Space Telescope. Objects at such distances would not normally be visible, providing information from further back in time than otherwise possible. Similarly, microlensing events can be used to obtain additional information about the source star. In addition to the greater brightness, limb darkening can be measured during high magnification events. If the source star is part of a binary system, the orbital motion of the source can sometimes be measured (called the xallarap effect, by analogy to parallax which is caused by the orbital motion of the Earth).

Observations of gravitational lensing can also be inverted to examine the lens itself. Direct measurements of the mass in any astronomical object are rare, and always welcome. Comparing mass and light typically involves assumptions about complicated astrophysical processes. Gravitational lensing is particularly useful if the lens is for some reason difficult to see. Gravitational microlensing can provide information on comparatively small astronomical objects, such as MACHOs (for Massive Astrophysical Compact Halo Object, such as brown dwarfs or large planets) within our own galaxy, or extrasolar planets (planets beyond the solar system). Strong and weak gravitational lensing of distant galaxies by foreground clusters can probe the amount and distribution of mass, which is dominated by invisible dark matter. The number of strong gravitational lenses throughout the sky can also be used to measure values of cosmological parameters such as the mean density of matter in the universe. Presently, the statistics do not place very strong limits on cosmological parameters, partly because the number of strong lenses found is relatively small. Weak gravitational lensing can extend the analysis away from these most massive clusters and, for example, reconstruct the large-scale distribution of mass, which is sensitive to cosmological parameters.

### ***1.3 Strong lensing***

The most spectacular manifestation of strong lensing is the formation of Einstein rings, which occurs when the source (such as a galaxy or star), the lens (such as another galaxy or a black hole) and observer are aligned. The first complete Einstein

ring, designated *B1998+666*, was discovered by collaboration between astronomers at the University of Manchester and NASA's Hubble Space Telescope in 1998.

The angular size of an Einstein ring is given by the Einstein radius. In radians, it is

$$\theta_E = \sqrt{\frac{4GM}{c^2} \frac{d_{LS}}{d_L d_S}}$$

where

$G$  is the gravitational constant,

$M$  is the mass of the lens,

$c$  is the speed of light,

$d_L$  is the observer-lens distance,

$d_S$  is the observer-source distance and

$d_{LS}$  is the lens-source distance.

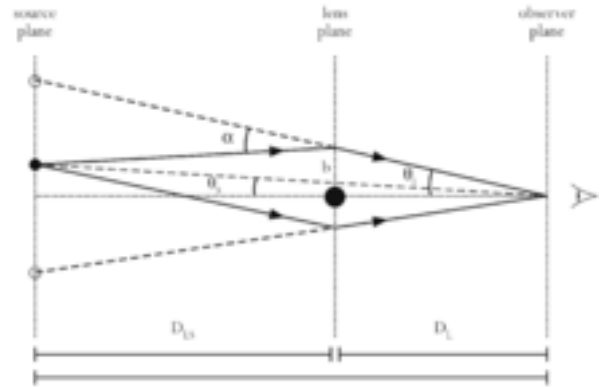


Figure 3. Gravitational lensing geometry.

Note that over cosmological distances,  $d_{LS} \neq d_S - d_L$  in general.

Most rings have first been discovered in the radio range. Out of hundreds of gravitational lenses, about half a dozen of them are partial Einstein rings with diameters up to an arc second. As either the mass distribution of the lenses is not perfectly axially symmetrical, or the source, lens and observer are not perfectly aligned, Einstein rings are rarely perfect. A collection of Einstein rings observed by the Hubble Space Telescope is displayed in Figure 4.

Using the Hubble Space Telescope (HST), a double ring has been found (Figure 5), arising from the light from three galaxies at distances of 3, 6 and 11 billion light years. Such rings help in understanding the distribution of dark matter, dark energy, the nature of distant galaxies, and the curvature of the universe. The odds of finding such a double ring are 1 in 10,000.

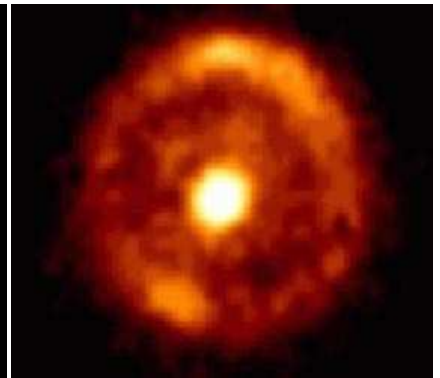
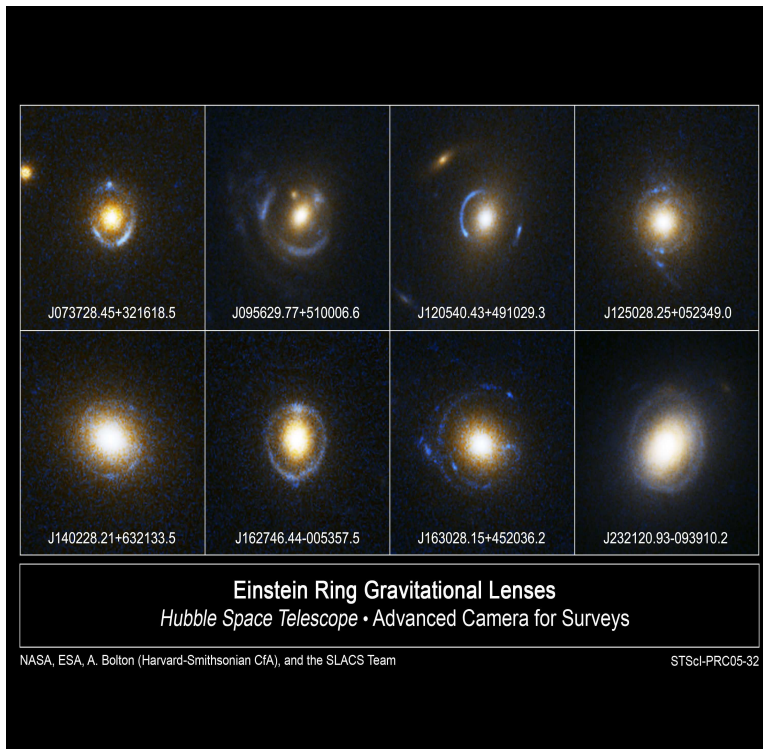


Figure 4. A collection of Einstein rings observed with the Hubble Space Telescope.

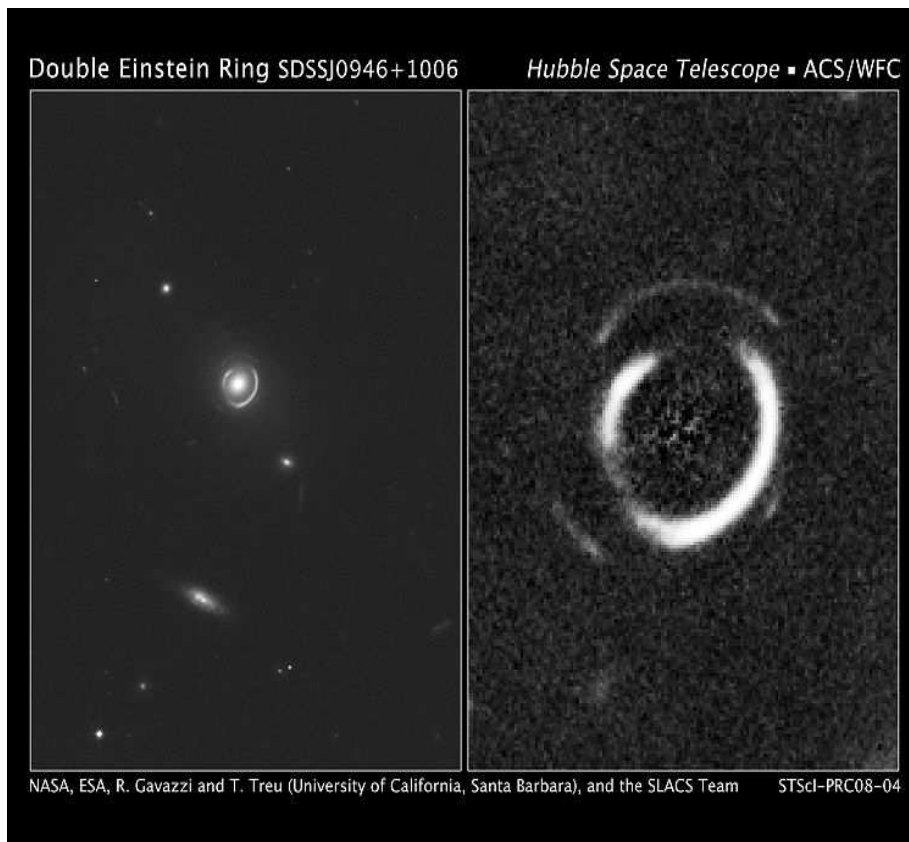


Figure 5. SDSSJ0946+1006 is a Double Einstein Ring. Credit: HST/NASA/ESA

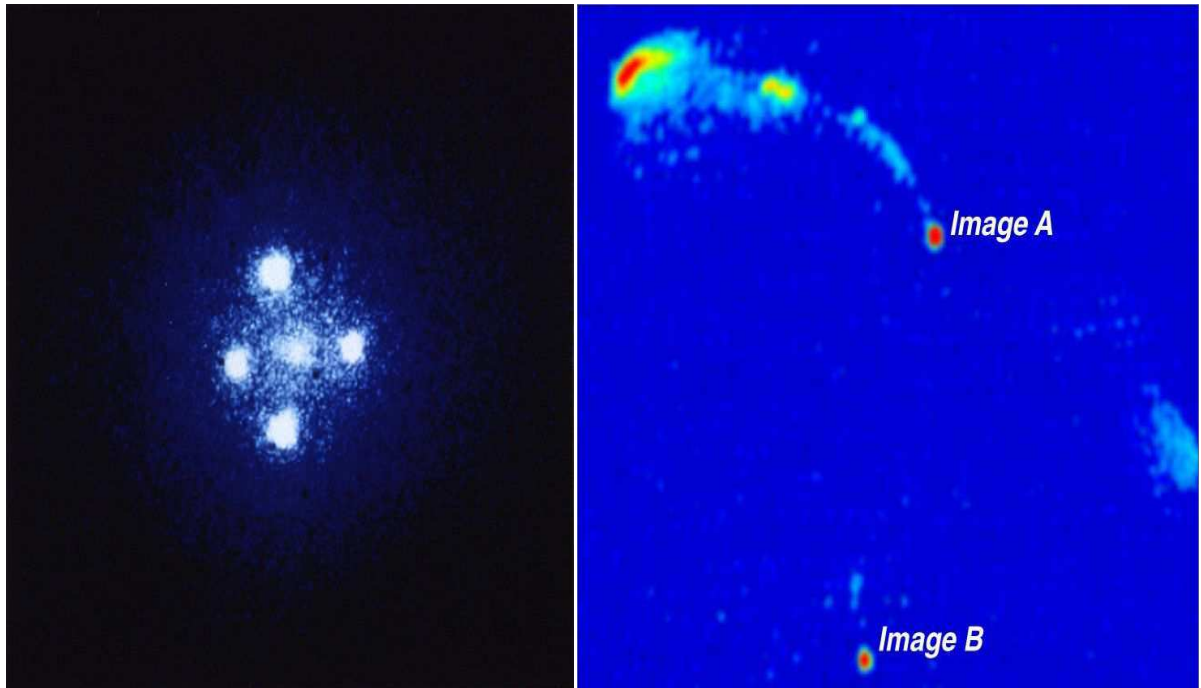


Figure 6. Examples of multiple images: the Einstein cross (left) and the Twin QSO (right).

Another manifestation of strong lensing is the formation of multiple images. The Einstein Cross ( $Q2237+0305$ ) is a gravitationally lensed quasar that sits directly behind ZW 2237+030, Huchra's Lens. Four images of the same distant quasar appear around a foreground galaxy due to strong gravitational lensing (Figure 6). The quasar is located about 8 billion light years from Earth, while the lensing galaxy is located at a

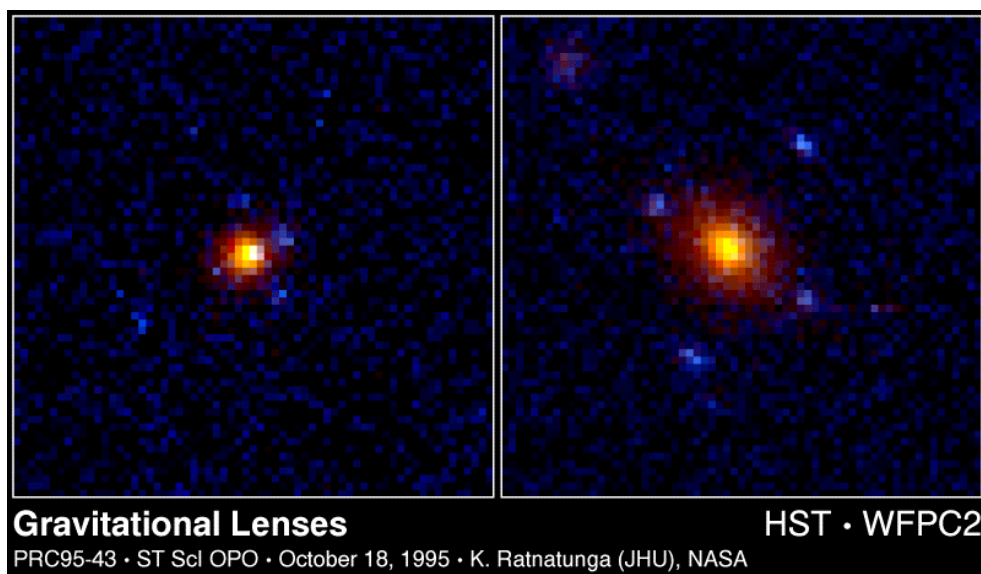


Figure 7. Other examples of multiple images seen by HST.

distance of 400 million light years. The apparent dimension of this galaxy is  $0.87 \times 0.34$  arc minutes, while the apparent dimension of the cross in its centre accounts for only  $1.6 \times 1.6$  arc seconds. The Einstein Cross can be found in Pegasus. Further examples of multiple images revealed by the HST are shown on Figure 7.

#### ***1.4 Weak lensing***

While the presence of any mass bends the path of light passing near it, this effect rarely produces the giant arcs and multiple images associated with strong lensing. Most lines of sight in the universe are in the weak lensing regime, in which the deflection is impossible to detect in a single background source. However, in such cases, the presence of the foreground mass can be detected by way of a systematic alignment of background sources around the lens. Weak gravitational lensing is thus an intrinsically statistical measurement, but it provides a way to measure the masses of astronomical objects without requiring assumptions about their composition or dynamical state.

The effect of gravitational lensing can be split into two terms, the convergence and shear. The convergence term magnifies the background objects by increasing their size, and the shear term stretches them tangentially around the foreground mass. To measure the tangential alignment, it is necessary to measure the ellipticities of the background galaxies and construct a statistical estimate of their systematic alignment. The fundamental problem is that galaxies are not intrinsically circular, so their measured ellipticity is a combination of their intrinsic ellipticity and the gravitational lensing shear. Typically, the intrinsic ellipticity is much greater than the shear (by a factor of 3-300, depending on the foreground mass). The measurements of many background galaxies must be combined to average down this “shape noise”. The orientation of intrinsic ellipticities of galaxies should be almost entirely random, so any systematic alignment between multiple galaxies can generally be assumed to be caused by lensing.

Another major challenge for weak lensing is correction for the point spread function (PSF) due to instrumental and atmospheric effects, which causes the observed images to be smeared relative to the “true sky”. This smearing tends to make small objects more round, destroying some of the information about their true ellipticity. As a

further complication, the PSF typically adds a small level of ellipticity to objects in the image, which is not at all random, and can in fact mimic a true lensing signal. Even for the most modern telescopes, this effect is usually at least the same order of magnitude as the gravitational lensing shear, and is often much larger. Correcting for the PSF requires building a model for how it varies across the field. Stars in our own galaxy provide a direct measurement of the PSF, and these can be used to construct such a model, usually by interpolating between the points where stars appear on the image. This model can then be used to reconstruct the “true” ellipticities from the smeared ones. Angular diameter distances to the lenses and background sources are important for converting the lensing observables to physically meaningful quantities. These distances are often estimated using known redshifts. Redshift information is also important in separating the background source population from other galaxies in the foreground, or those associated with the mass responsible for the lensing.

Of particular interest is the case of galaxy clusters, which are among the largest gravitationally bound structures in the Universe, surpassed only by superclusters, with approximately 80% of cluster content in the form of dark matter. The gravitational fields of these clusters deflect light-rays travelling near them, possibly causing dramatic distortions by strong lensing, such as multiple images, arcs, and rings (Figure 8).

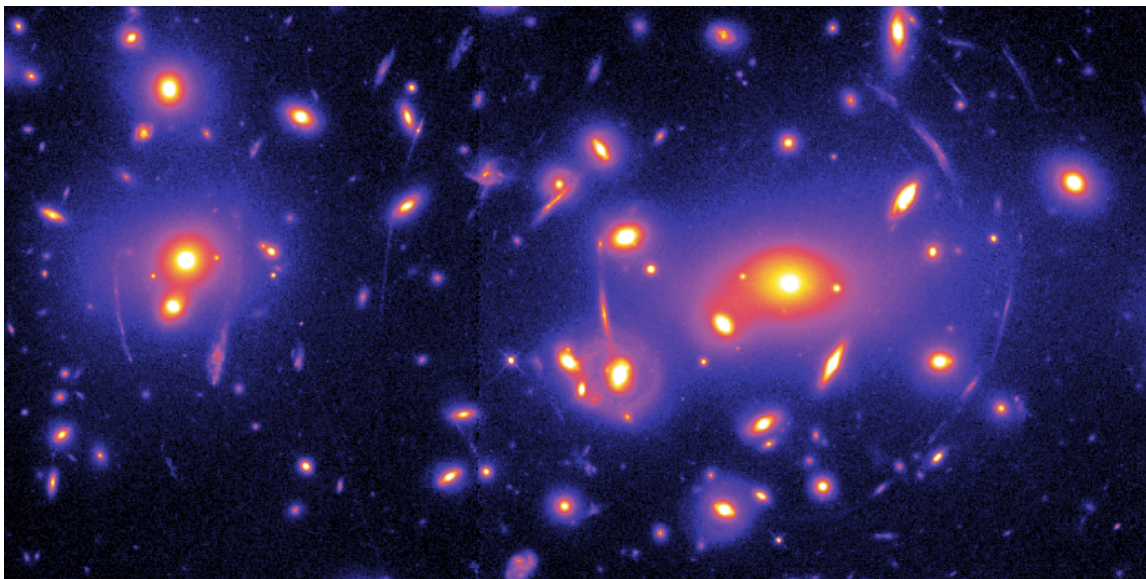


*Figure 8. A distant galaxy lensed by Cluster Abell 2218.*

More generally, the effect causes small, but statistically coherent, distortions of background sources on the order of 10% by weak lensing.

The projected mass density can be recovered from the measurement of the ellipticities of the lensed background galaxies. However, a mass distribution reconstructed without knowledge of the magnification suffers from a limitation known as the mass sheet degeneracy. It can be lifted using an independent measurement of the magnification. The cluster centre is determined by using a reconstructed mass distribution or optical or X-ray data. Knowledge of the lensing cluster redshift and the redshift distribution of the background galaxies is also necessary. Individual mass estimates from weak lensing can only be derived for the most massive clusters, and the accuracy of these mass estimates are limited by projections along the line of sight.

Cluster mass estimates determined by lensing are valuable because the method requires no assumption about the dynamical state or star formation history of the cluster. Lensing mass maps can also potentially reveal "dark clusters," clusters containing overdense concentrations of dark matter but relatively insignificant amounts of normal matter. Comparison of the dark matter distribution mapped using lensing with the normal matter distribution mapped using optical and X-ray data reveals the interplay of the dark matter with the stellar and gas components. A notable example of such a joint analysis is the so-called Bullet Cluster (Figure 9).

Another interesting case of weak (and occasionally strong) lensing is galaxy-galaxy lensing in which the foreground object responsible for distorting the shapes of background galaxies is itself an individual galaxy (as opposed to a galaxy cluster). It produces shear correlations of  $\sim 1\%$ , weaker than the signal due to cluster lensing.

J.A. Tyson and collaborators had first postulated the concept of galaxy-galaxy lensing in 1984, but the observational results of their study were inconclusive. It was not until 1996 that evidence of such distortion was tentatively discovered, with the first statistically significant results not published until the year 2000. Since those initial discoveries, the construction of larger, high resolution telescopes and the advent of dedicated wide field galaxy surveys have greatly increased the observed number density of both background source and foreground lens galaxies, allowing for a much

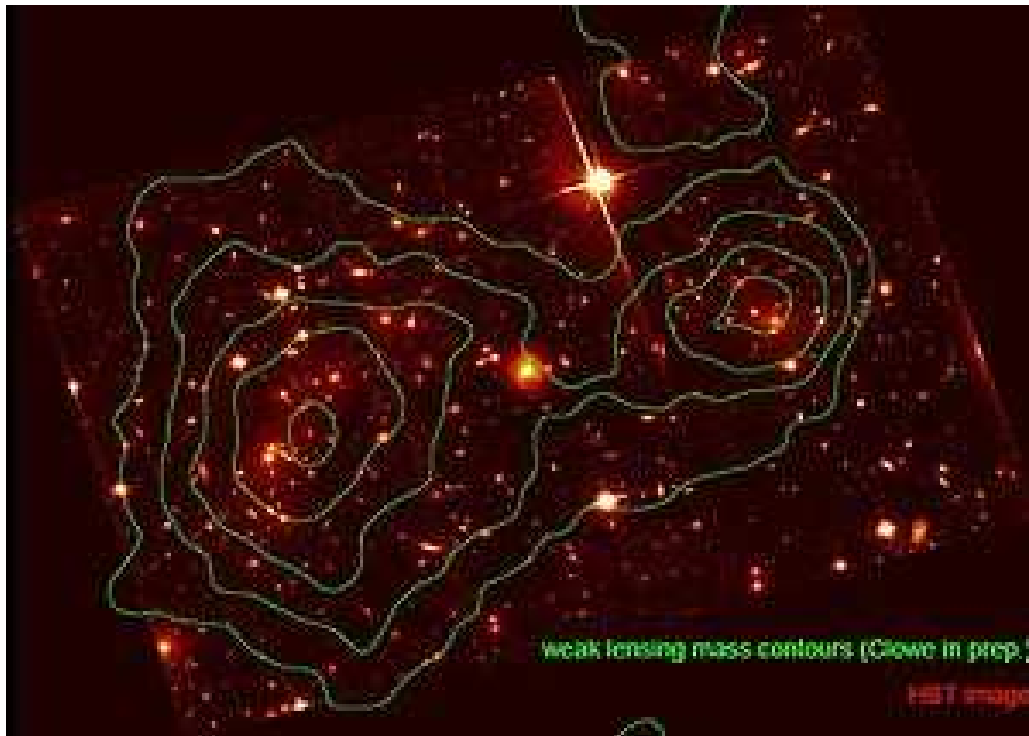


*Figure 9. Image of the Bullet Cluster from the Hubble Space Telescope with total mass contours (dominated by dark matter) from a lensing analysis overlaid.*

more robust statistical sample of galaxies, making the lensing signal much easier to detect. Today, measuring the shear signal due to galaxy-galaxy lensing is a widely used technique in observational astronomy and cosmology, often used in parallel with other measurements in determining physical characteristics of foreground galaxies.

Due to the relatively low mass of field lenses and the inherent randomness in intrinsic shape of background sources, the signal is impossible to measure on a galaxy by galaxy basis and must be obtained by combining the signals of many individual lens measurements together (a technique known as “stacking”). Galaxy-galaxy lensing is used to measure galaxy mass density profiles (from the central cores of galaxies where normal matter dominates to the outer halo where dark matter dominates). Comparing the measured mass to the luminosity in a specific filter, galaxy-galaxy lensing can also provide insight into the mass to light ratios of field galaxies. Galaxy mass evolution can also be studied by restricting the lens sample of a galaxy-galaxy lensing study to lie at only one particular redshift. Finally, gravitational lensing by large-scale structure also produces an observable pattern of alignments in background galaxies, but

this distortion is only  $\sim 0.1\%$ - $1\%$  - much more subtle than cluster or galaxy-galaxy lensing. It was not until 2000 that four independent groups published the first detections of cosmic shear. Subsequent observations have started to put constraints on cosmological parameters that are competitive with other cosmological probes.

Weak lensing also has an important effect on the Cosmic Microwave Background (CMB) and diffuse 21 cm line radiation.

### ***1.5 Microlensing***

Microlensing is caused by the same physical effect as strong lensing and weak lensing, but it is studied using very different observational techniques. In strong and weak lensing, the mass of the lens is large enough for the displacement of light by the lens to be resolved with a high-resolution telescope such as the HST. With microlensing, the lens mass is too low (a planet or a star) for the displacement of light to be observed easily, but the apparent brightening of the source may still be detected. In such a situation, the lens will pass by the source in a reasonable amount of time, seconds to years instead of millions of years. As the alignment changes, the source's apparent brightness changes, and this can be monitored to detect and study the event. Thus, unlike with strong and weak gravitational lenses, a microlensing event is a transient phenomenon. Unlike with strong and weak lensing, no single observation can establish that microlensing is occurring. Instead the rise and fall of the source brightness must be monitored over time using photometry. The function of brightness versus time is known as a light curve. A typical microlensing light curve (Figure 10) has a very simple shape, and only one physical parameter can be extracted: the time scale, which is related to the lens mass, distance, and velocity. There are several effects, however, that contribute to the shape of more atypical lensing events. If the lens mass is not concentrated in a single point, the light curve can be dramatically different and may exhibit strong spikes in the light curve, as can be seen when the lens is a binary star or a planetary system. In extremely bright or quickly changing microlensing events, the source star cannot be treated as an infinitesimally small point of light: the size of the star's disk matters. For events

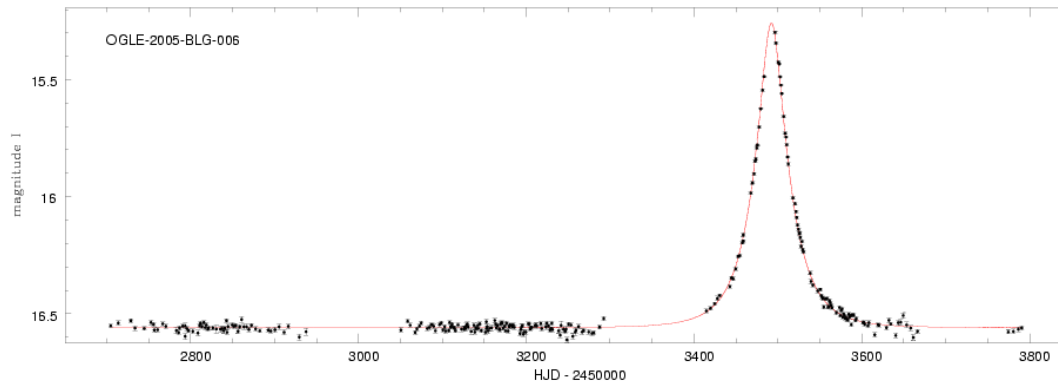


Figure 10. A typical microlensing event (OGLE, 2005).

lasting for months, the motion of the Earth around the Sun can cause the alignment to change slightly, affecting the light curve.

Most focus is currently on the more unusual microlensing events, especially those that might lead to the discovery of extra solar planets (so-called exoplanets). In practice, because the alignment needed is so precise and difficult to predict, microlensing is very rare. Events, therefore, are generally found with surveys, which photometrically monitor tens of millions of potential source stars, every few days for several years. Dense background fields suitable for such surveys are nearby galaxies, such as the Magellanic Clouds and the Andromeda galaxy, and the Milky Way bulge. In each case, the lens population studied comprises the objects between Earth and the source field: for the bulge, the lens population is the Milky Way disk stars, and for external galaxies, the lens population is the Milky Way halo, as well as objects in the other galaxy itself. The density, mass, and location of the objects in these lens populations determine the frequency of microlensing along the line of sight, which is characterized by a value known as the optical depth due to microlensing. The optical depth is, roughly speaking, the average fraction of source stars undergoing microlensing at a given time, or equivalently the probability that a given source star is undergoing lensing at a given time. The MACHO project found the optical depth toward the LMC to be  $1.2 \times 10^{-7}$  or about 1 in 8,000,000, and the optical depth toward the bulge to be  $2.43 \times 10^{-6}$  or about 1 in 400,000.

Complicating the search is the fact that for every star undergoing microlensing, there are thousands of stars changing in brightness for other reasons (about 2% of the

stars in a typical source field are naturally variable stars) and other transient events (such as novae and supernovae), and these must be weeded out to find true microlensing events. After a microlensing event in progress has been identified, the monitoring program that detects it often alerts the community to its discovery, so that other specialized programs may follow the event more intensively, hoping to find interesting deviations from the typical light curve. This is because these deviations – particularly those due to exoplanets – require hourly monitoring to be identified, which the survey programs are unable to provide while still searching for new events. The question of how to prioritise events in progress for detailed follow-up with limited observing resources is very important for microlensing researchers today.

Gravitational lensing was first observed in 1979, in the form of a quasar lensed by a foreground galaxy. That same year, Kyongae Chang and Sjur Refsdal showed that individual stars in the lens galaxy could act as smaller lenses within the main lens, causing the source quasar's images to fluctuate on a timescale of months. Bohdan Paczyński first used the term “microlensing” to describe this phenomenon. This type of microlensing is difficult to identify because of the intrinsic variability of quasars, but in 1989 Mike Irwin and collaborators published detection of microlensing in Huchra's Lens.

In 1986, Paczyński proposed using microlensing to look for dark matter in the form of massive compact halo objects (MACHOs) in the Galactic halo, by observing background stars in a nearby galaxy. Two groups of particle physicists working on dark matter heard his talks and joined with astronomers to form the Anglo-Australian MACHO collaboration and the French EROS collaboration. In 1991 Paczyński suggested that microlensing might be used to find planets, and in 1992 he founded the OGLE microlensing experiment, which began searching for events in the direction of the Galactic bulge.

The first two microlensing events in the direction of the Large Magellanic Cloud that might be caused by dark matter were reported in back to back Nature papers by MACHO and EROS in 1993, and in the following years, events continued to be detected. The MACHO collaboration ended in 1999. Their data refuted the hypothesis that 100% of the dark halo comprises MACHOs, but they found a significant unexplained excess of roughly 20% of the halo mass, which might be due to MACHOs

or to lenses within the Large Magellanic Cloud itself. EROS subsequently published even stronger upper limits on MACHOs. Despite not solving the dark matter problem, microlensing has been shown to be a useful tool for many applications. Hundreds of microlensing events are detected per year toward the Galactic bulge, where the microlensing optical depth (due to stars in the Galactic disk) is about 20 times greater than through the Galactic halo. In 2007, the OGLE project identified 611 event candidates, and the MOA project (a Japan-New Zealand collaboration) identified 488 (although not all candidates turn out to be microlensing events, and there is a significant overlap between the two projects). In addition to these surveys, follow-up projects are underway to study in detail potentially interesting events, primarily with the aim of detecting extra solar planets.

In typical microlensing events, the Einstein radius is so small that it is not generally observed, but it can be observed in some extreme events as described below.

During a microlensing event, the brightness of the source is amplified by a factor  $A$ , which is expressed as a function of a dimensionless number  $u$ , defined as the angular separation of the lens and the source divided by the Einstein radius, as shown below:

$$A(u) = \frac{u^2 + 2}{u\sqrt{u^2 + 4}}$$

This function has several important properties.  $A(u)$  is always greater than unity, so microlensing can only increase the brightness of the source star, not decrease it.  $A(u)$  always decreases as  $u$  increases, so the closer the alignment, the brighter the source becomes. As  $u$  approaches infinity,  $A(u)$  approaches 1, so that at wide separations, microlensing has no effect. Finally, as  $u$  approaches 0,  $A(u)$  approaches infinity as the images approach an Einstein ring. For perfect alignment ( $u = 0$ ),  $A(u)$  is theoretically infinite. In practice, finite source size effects will set a limit to how large an amplification can occur for very close alignment, but some microlensing events can cause a brightening by factors of hundred.

Unlike in strong or weak lensing, where the lens is a galaxy or cluster of galaxies, in microlensing  $u$  changes significantly in a short period of time. The relevant

time scale is called the Einstein time  $t_E$ , and is given by the time it takes the lens to traverse an angular distance of one Einstein radius. For typical microlensing events,  $t_E$  is on the order of a few days to a few months.

$$u(t) = \sqrt{u_{min}^2 + \left(\frac{t - t_0}{t_E}\right)^2}$$

The minimum value of  $u$ , called  $u_{min}$ , determines the peak brightness of the event.

In a typical microlensing event, the light curve is well fit by assuming that the source is a point, the lens is a single point mass, and the lens is moving in a straight line. In these events, the only physically significant parameter that can be measured is the Einstein timescale  $t_E$ . Since this observable is a degenerate function of the lens mass, distance, and velocity, one cannot determine these physical parameters from a single event. However, in some cases, events can be analysed to yield the additional parameters of the Einstein angle and parallax. These include very high magnification events, binary lenses, parallax and xallarap events, and events where the lens is visible.

Although the Einstein angle is too small to be directly visible from a ground-based telescope, several techniques have been proposed to observe it.

In rare cases, when the lens passes directly in front of the source star, the finite size of the source star becomes an important parameter. These measurements require an extreme alignment between source and lens.

If the lens is a binary star with separation of roughly the Einstein radius, the magnification pattern is more complex than in the single star lenses. In this case, there are typically three images when the lens is distant from the source, but there is a range of alignments where two additional images are created. These alignments, known as *caustics*, produce very high magnifications and may some time be used to measure the Einstein radius.

In principle, the Einstein parallax can be measured by two observers simultaneously observing the event from different locations, e.g. from the earth and from a distant spacecraft, and comparing the amplifications that they observe. Such a direct measurement was recently reported using the Spitzer Space Telescope. More

typically, the Einstein parallax is measured from the non-linear motion of the observer caused by the rotation of the Earth about the Sun. It was first reported in 1995 and has been reported in a handful of events since.

If the source star is a binary star, then it too will have a non-linear motion which can also cause slight, but detectable changes in the light curve. This effect is known as *Xallarap* (parallax spelled backwards).

If the lensing object is a star with a planet orbiting it (Figure 11), this is an extreme example of a binary lens event. If the source crosses a caustic, the deviations from a standard event can be large even for low mass planets. These deviations allow one to infer the existence and determine the mass and separation of the planet around the lens. Deviations typically last a few hours or a few days. Because the signal is strongest when the event itself is strongest, high-magnification events are the most promising candidates for detailed study. Typically, a survey team notifies the community when they discover a high-magnification event in progress. Follow-up groups then intensively monitor the ongoing event, hoping to get good coverage of the deviation if it occurs. When the event is over, the light curve is compared to theoretical models to find the physical parameters of the system. The parameters that can be determined directly from this comparison are the mass ratio of the planet to the star, and the ratio of the star-planet angular separation to the Einstein angle. From these ratios, along with assumptions about the lens star, the mass of the planet and its orbital distance can be estimated. The first success of this technique occurred in 2003 by both OGLE and MOA of the microlensing event OGLE 2003-BLG-235 (or MOA 2003-BLG-53). Combining their data, they found the most likely planet mass to be 1.5 times the mass of Jupiter. As of January 2011, eleven exoplanets have been detected by this method. Notably, at the time of its announcement in January 2006, the planet OGLE-2005-BLG-390Lb probably had the lowest mass of any known exoplanet orbiting a regular star, with a median at 5.5 times the mass of the Earth and roughly a factor two uncertainty. This record was contested in 2007 by Gliese 581 c with a minimal mass of 5 Earth masses, and since 2009 Gliese 581 e is the lightest known "regular" exoplanet, with minimum 1.9 Earth masses. Figure 12 illustrates the progress achieved.

Comparing this method of detecting extrasolar planets with other techniques such as the transit method, one advantage is that the intensity of the planetary deviation

does not depend on the planet mass as strongly as effects in other techniques do. This makes microlensing well suited to finding low-mass planets. One disadvantage is that follow-up of the lens system is very difficult after the event has ended, because it takes a long time for the lens and the source to be sufficiently separated to resolve them separately.

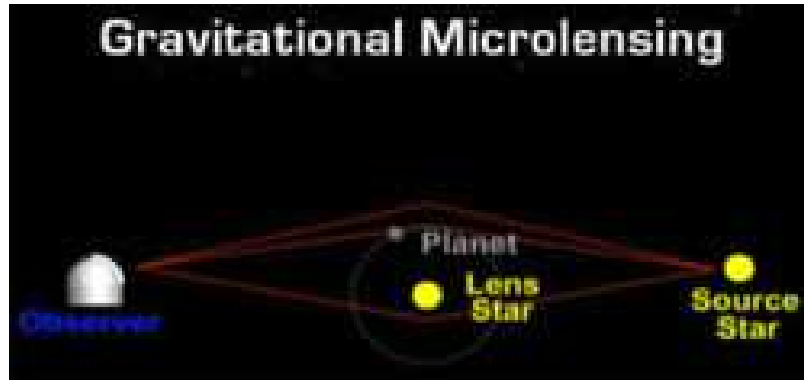


Figure 11. Detection of exoplanets by gravitational microlensing.

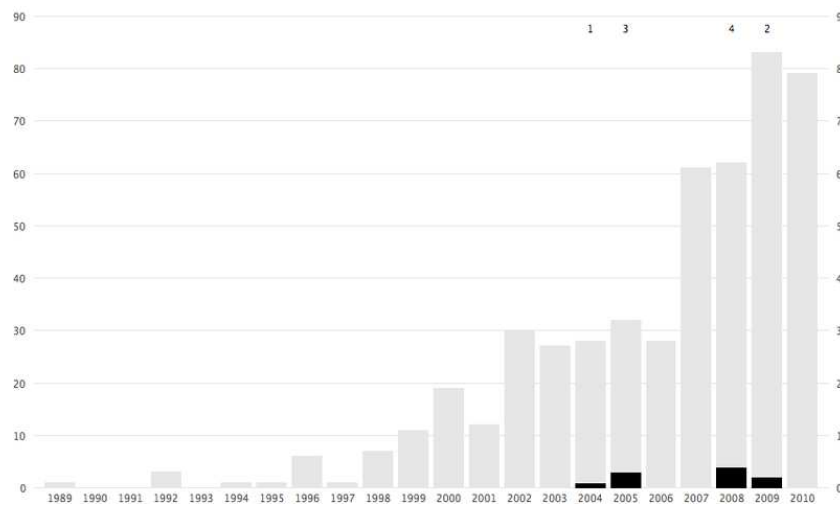


Figure 12. Exoplanets discovered using microlensing, by year, through 2010-01

## 2. Theoretical basis

### 2.1 Special relativity

A brief reminder of the bases of special relativity is necessary to introduce what it implies when dealing with gravitation. Unless otherwise specified we use natural units where  $\hbar = c = 1$ .

The basis of special relativity is the so-called relativity principle according to which the laws of nature are the same in two frames in uniform movement with respect to each other, usually referred to as inertial frames. The movements in two such frames are related by the so-called Lorentz transformation.

Lorentz transformations along  $Ox$  read ( $y$  and  $z$  being unchanged)

$$x' = x \cosh\alpha + t \sinh\alpha$$

$$t' = x \sinh\alpha + t \cosh\alpha$$

The system  $S$  in which  $x$  and  $t$  are measured moves along the  $x$  axis, which is the same as the  $x'$  axis, with velocity  $\beta = \tanh\alpha$  measured in the system  $S'$  where  $x'$  and  $t'$  are measured.

In  $S'$  two events measured at a same time  $t'$  give

$$(x_1 - x_2) \sinh\alpha + (t_1 - t_2) \cosh\alpha = 0 \text{ and therefore}$$

$$\begin{aligned} x'_1 - x'_2 &= (x_1 - x_2) \cosh\alpha + (t_1 - t_2) \sinh\alpha \\ &= (x_1 - x_2) (\cosh\alpha - \sinh^2\alpha / \cosh\alpha) \\ &= (x_1 - x_2) / \cosh\alpha. \end{aligned}$$

Namely **distances** appear to be **contracted** by a factor  $\gamma = \cosh\alpha = 1/\sqrt{1-\beta^2}$ .

On the contrary, two events measured at a same location  $x$  in  $S$  give

$t'_1 - t'_2 = (t_1 - t_2) \cosh\alpha$ . Namely **time differences** appear to be **dilated** by the same factor  $\gamma$ .

This result is not as trivial as it may sound, as it might seem to introduce an asymmetry between  $S$  and  $S'$ . Superficially, one might think that distances measured in  $S$  will appear dilated with respect to  $S'$  and that time differences measured in  $S$  will

appear contracted, but it is not true of course. It is the measurement process that is not symmetric: to measure a distance in the fixed frame you compare two events that occur at the same time in the fixed frame while to measure a time difference in the fixed frame you compare two events that occur at the same location in the moving frame. It is important to have well understood this somewhat subtle difference.

As  $\exp(\pm i\alpha) = \cos(\alpha) \pm i \sin(\alpha)$ ,  $\cos(\alpha) = \{\exp(i\alpha) + \exp(-i\alpha)\}/2 = \cosh(i\alpha)$  and  $\sin(\alpha) = \{\exp(i\alpha) - \exp(-i\alpha)\}/2i = -i \sinh(i\alpha)$ . The Lorentz transformation may therefore be rewritten, replacing  $\cosh\alpha$  by  $\cos(-i\alpha)$  and  $\sinh(\alpha)$  by  $i \sin(-i\alpha)$

$$x' = x \cos(i\alpha) - it \sin(i\alpha)$$

$$it' = x \sin(i\alpha) + it \cos(i\alpha)$$

A Lorentz transformation is therefore a rotation by an angle  $i\alpha$  in the  $(x, it)$  plane. In the same way as a rotation in the  $(x, y)$  plane leaves  $x^2 + y^2$  invariant, the Lorentz transformation leaves  $x^2 + (it)^2 = x^2 - t^2$  invariant. And in the same way as the rotation by an angle  $\alpha$  simply increases the polar angle  $\theta$  of the vector  $(x, y)$  by  $\alpha$ , the Lorentz transformation increases by  $i\alpha$  the equivalent of  $\theta$ , which can be written as  $\text{atan}(it/x) = i \text{argth}(t/x)$ . The quantity  $\text{argth}(t/x)$ , which increases by  $\alpha$  in the Lorentz transformation, may also be written<sup>1</sup>  $1/2 \ln \{(t+x)/(t-x)\}$ . When referred to the energy-momentum four vector, this quantity is called *rapidity*.

If a velocity  $v_x = dx/dt$  parallel to  $Ox$  is measured in  $S$ , the velocity  $v_x' = dx'/dt'$  measured in  $S'$  is  $(dx \cosh\alpha + dt \sinh\alpha)/(dx \sinh\alpha + dt \cosh\alpha) = (v_x + \beta)/(1 + \beta v_x)$ . One recognizes here the law of addition of  $\tanh$ , the product of two rotations being a rotation by the sum of the rotation angles. Whatever  $v_x < 1$  and  $\beta < 1$ ,  $v_x'$  is still a  $\tanh$  and always smaller than 1: the light velocity cannot be exceeded by adding velocities that are themselves smaller than the light velocity. However one may conceive the existence of particles having velocities larger than the light velocity, such particles have received a name, *tachyons*, even though no evidence for them has ever been found. If a velocity  $v_y = dy/dt$  normal to  $Ox$  is measured in  $S$ , the velocity  $v_y' = dy'/dt'$  measured in  $S'$  is  $dy/(dx \sinh\alpha + dt \cosh\alpha) = v_y/[\gamma(1 + \beta v_x)]$ . Note that  $v_y'/v_x' = v_y/[\gamma(v_x + \beta)]$

---

<sup>1</sup> Indeed  $\tanh(1/2 \ln \{(t+x)/(t-x)\})$   
 $= \{\exp[1/2 \ln \{(t+x)/(t-x)\}] - \exp[-1/2 \ln \{(t+x)/(t-x)\}]\} / \{\exp[1/2 \ln \{(t+x)/(t-x)\}] + \exp[-1/2 \ln \{(t+x)/(t-x)\}]\} = \{\sqrt{(t+x)/(t-x)} - \sqrt{(t-x)/(t+x)}\} / \{\sqrt{(t+x)/(t-x)} + \sqrt{(t-x)/(t+x)}\} = (t+x-t-x)/(t+x+t-x) = x/t$ .

and  $v'^2 = v_x'^2 + v_y'^2 = (v_x^2 + 2\beta v_x + \beta^2 + v_y^2 - \beta^2 v_y^2) / (1 + \beta v_x)^2$ . Writing  $v^2 = v_x^2 + v_y^2$  we find  $v'^2 - 1 = (v^2 - 1)(1 - \beta^2) / (1 + \beta v_x)^2$ . In particular, as  $v'^2 - 1$  and  $v^2 - 1$  have the same sign, velocities smaller than the light velocity remain so and  $v = 1$  implies  $v' = 1$ .

Finally, let us recall that energy  $E$  and momentum  $\mathbf{p}$  form a four vector, implying that  $E^2 - \mathbf{p}^2 = m^2$ ,  $m$  being the rest mass of the particle, a scalar. Its rapidity (measured along  $Ox$ ), as was already said, is  $y = \frac{1}{2} \ln \{ (E + p_x) / (E - p_x) \}$ . The leading terms of the development of  $E$  and  $\mathbf{p}$  are  $E = m + \frac{1}{2} m v^2$  and  $\mathbf{p} = m \mathbf{v}$ .

### 2.2 Gravity of photons

The idea that gravity can be described as a geometric property of space-time rather than as a dynamical process is at the root of general relativity. It makes an elegant use of a remark – which was made at Galileo time but had not yet been made use of – that all masses fall in the same way in a gravity field. In Newtonian language this implies that the inertial and gravitational masses are equal<sup>2</sup> and are irrelevant to energy conservation: both the gravity potential and the kinetic energy are proportional to it. The extension of the relativity principle from inertial frames to free falling frames allows for describing locally, in any small space-time domain, the gravity field by an adequate acceleration given to the free-falling frame. Without going much further into the mathematics implied by these statements, one can deduce a host of important consequences touching the need for a revision of our concepts of space and time and for giving up special relativity, retaining it only locally.

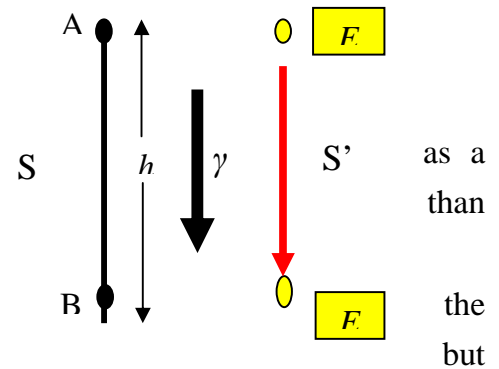


Figure 13. Gravity of photons

<sup>2</sup> The first accurate measurement of the equality of the inertial and gravitational masses was due to Roland von Eötvös. It was later considerably improved by Robert H. Dicke and Vladimir B. Braginskii in the gravity field of the Sun and, more recently, by Eric G. Adelberger. The two masses are known to be equal to within  $10^{-12}$ . A very precise analysis of the relative motion of the Moon with respect to the Earth, using laser reflectors left on the Moon by Apollo 11, 14 and 15 and Linnakhod 2, has shown that the gravitational binding energy contributes identically to the inertial and gravitational masses.

As a very simple illustration, consider a homogeneous gravity field directed along  $Oz$  in  $S$ . Let  $\gamma$  be the acceleration (Figure 13). In the free falling frame  $S'$  defined by the transformation  $z' = z - 1/2\gamma t^2$  all masses have a uniform linear movement. Extending the principle of relativity to this free falling frame we obtain a number of interesting results.

Take two points in  $S$ ,  $A$  and  $B$ , on top of each other,  $A$  above  $B$  at a distance  $h$  from it. Send a photon of energy  $E$  from  $A$  to  $B$ . In  $B$ , the photon has an energy  $E'$ , which would be equal to  $E$  if the gravity field had no action on massless particles. To evaluate it consider the event in the free falling frame  $S'$  where the gravitational field vanishes. This system starts at zero velocity from  $A$  and reaches a velocity  $\gamma t$  in  $B$ , with  $t=h$  being the time it took for the photon to go from  $A$  to  $B$ . A photon being massless has equal energy and momentum,  $E=p$ . At  $B$ , the Lorentz transformation reads  $E' = \cosh\alpha E + \sinh\alpha p$  where  $\tanh\alpha = \gamma h$ . To first order in  $\alpha$ ,  $E' = E + E\gamma h$ , namely the photon has acquired an additional energy  $E\gamma h$  in the gravity field, corresponding to the usual  $m_0\gamma h$  term in classical Newton mechanics,  $m_0$  being the rest mass. It is indeed  $E$  and not  $m_0$  that matters, it is energy that weighs, not rest mass<sup>3</sup>. Accordingly, when a star having a mass  $M$  and a radius  $R$  emits a photon of frequency  $\nu$ , this photon is red shifted when it reaches far distances by an amount (remember that  $E = \hbar\nu$ )  $\Delta\nu/\nu = \Delta E/E = \gamma R = GM/R$ . One speaks of a gravitational red shift<sup>4</sup>. In the case of the Sun, the radius is 110 times larger than the Earth radius but the density is 4 times smaller, hence  $\gamma$  is 27 times larger, that is  $0.27 \text{ km/s}^2$  and  $\Delta\nu/\nu = 0.27 \times 110 \times 6400 / (3 \cdot 10^5)^2 = 2 \cdot 10^{-6}$ . In the case of a neutron star  $\Delta\nu/\nu$  may take values of order unity, in which case this first order estimate is no longer valid.

---

<sup>3</sup> While  $m_0$  was a scalar,  $E$  is not: gravity is not a scalar field.  $E$  is the fourth component of a four-vector, implying that gravity is in fact a tensor field: we will have to consider the energy-momentum tensor to describe what gravity couples to in the general case of a non uniform gravity field. At the end of the XIX<sup>e</sup> century, with the success of Maxwell equations, and even shortly after special relativity, many tried to describe gravity as a vector field but it had to fail. The carrier of gravity, the so-called graviton, has accordingly spin 2.

<sup>4</sup> Gravitational red shift on Earth ( $10^{-16}$  per meter!) has been measured using the Mössbauer effect by Robert V. Pound and his colleagues to an accuracy of one percent. Using a hydrogen maser clock in a rocket at 10 000 km altitude, Robert F. C. Vessot and collaborators have measured the gravitational red shift to an accuracy of 2 parts in  $10^4$ .

### 2.3 Schwarzschild metric

Another way to look at the action of gravity on photons is to consider a mass  $M$  isolated in space, a star or a galaxy, and compare two different free falling frames: one has just enough velocity to escape to infinity, namely its metric is defined by the normal special relativity metric,  $ds^2 = dt^2 - dl^2$ ; the other has less, enough to reach a distance  $r$  from  $M$ , at which point its velocity cancels and it falls back onto  $M$ . The timing is such that the first frame coincides with the second at the very moment where the latter has reached its turning point. The velocity  $V$  of the first frame at this moment is the escape velocity at  $r$ , such that  $1/2V^2 = MG/r$ , that is  $V = \sqrt{2MG/r}$  (we assume that  $r$  is large enough for  $V$  to be much smaller than  $c$  and Newtonian arithmetic to apply). The metric in the second frame is trivially obtained from that in the first frame by Lorentz transformation: distances are contracted and times dilated by a same factor,  $1/\sqrt{1-V^2} = 1/\sqrt{1-2MG/r}$ . Hence the metric in the second frame:  $ds^2 = (1-2MG/r)dt^2 - (1-2MG/r)^{-1}dr^2$ . It is called the Schwarzschild metric. Introducing the polar angles  $\theta$  and  $\varphi$ , which are unaffected, it reads:

$$ds^2 = (1-2MG/r)dt^2 - (1-2MG/r)^{-1}dr^2 - r^2(\sin^2\theta d\varphi^2 + d\theta^2).$$

A singularity occurs at  $R_{Schwarzschild} = 2MG$ , the Schwarzschild radius, where the escape velocity is equal to the light velocity (equivalently, where a body falling from infinity, originally with zero velocity, has been accelerated to the light velocity). It corresponds to black holes.

The Schwarzschild metric, written here in the case of a single mass isolated in space, is in fact valid in a much more general case: Birkhoff has shown that Schwarzschild's metric holds in empty space surrounding any spherically symmetric mass distribution, even if this empty space is itself embedded in a larger, spherically symmetric distribution of matter.

## 3. Bending of light

### 3.1 Gravitational delay

Consider light travelling from the surface of the Sun to the Earth, namely  $ds = d\theta = d\varphi = 0$ . Then  $dt = dr/(1-2MG/r)$ . The time  $t$  taken by the light to reach the Earth is therefore  $\int dr/(1-2MG/r) = \int r dr/(r-2MG) = \int (u+2MG)du/u$  where  $u = r-2MG$ .

Hence  $t=t_0+2MG\ln\{(a_{earth}-2MG)/(R_{sun}-2MG)\}$  where  $t_0$  is the time in the absence of gravity,  $a_{earth}$  is the radius of the Earth orbit and  $R_{sun}$  is the Sun radius. Putting numbers in gives a gravitational delay of the order of  $50 \mu s$ , namely  $10^{-7}$  times the uncorrected time. When sending a radar signal from the Earth to Venus and back, one may compare the extreme situations where Venus is on the other side or on the same side as the Earth with respect to the Sun, almost lined up in both cases. Then the difference in travel time corresponds to two full traversals near the Sun, namely  $4 \times 50 = 200 \mu s$ . This has been verified with a precision of the order of a percent. The above calculation neglected the delay experienced by the photons when passing by the Sun because of their angular deviation. To estimate it, we set  $ds=dr=d\theta=0$  and  $\theta=\pi/2$  in the Schwarzschild metric. Hence,  $dt=r d\phi/(1-2MG/r)$ . Putting numbers in, it corresponds to less than 10% of the gravitational delay calculated above.

### 3.2 Gravitational lensing

The gravitational delay for a far away star seen near the Sun edge (Figure 14) is twice that given above for the gravitational delay from the Sun to the Earth, namely  $\Delta t=4MG\ln(R-2MG) +$  terms that do not depend on  $R$ . Taking the derivative, we obtain  $d(\Delta t)/dR \sim -4MG/R$ ,  $R$  being now the closest distance of approach to the Sun. This measures the angle by which the wave front planes are bent when passing near the Sun, which is also the angle by which the light rays are bent since they are normal to the wave fronts. It corresponds to nearly 2 seconds of arc, which is a measurable quantity.

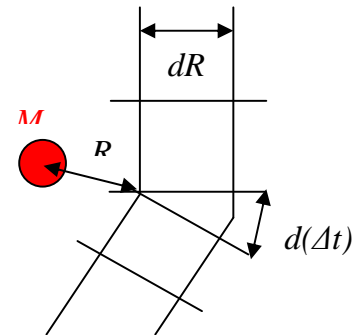


Figure 14. Gravitational lensing

The Sun may be thought of as being a weak lens with focal length equal to its radius divided by this angle of deflection, namely some 550 AU. As we saw in the introduction, such gravitational lensing effects are seen in many instances; in particular they may produce so called *Einstein rings* on very distant quasars. It is important to note that the bending of light is independent from the light frequency and applies equally not only to visible lights of different colours (Figure 15) but also to radio waves and X-rays.

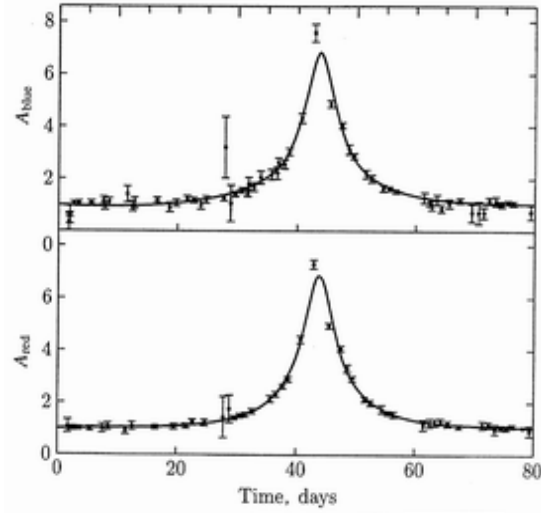


Figure 15. Gravitational microlensing in two different colors showing the increase of luminosity of a LMC (Large Magellanic Cloud) star in the background resulting from the passage in front of it of an obscure object in the halo of our galaxy.

Rather than calculating the total deviation experienced by light from infinity to infinity when passing by a massive object, let us calculate the form taken by the differential bending angle at a distance  $r$  from the center of the massive object (the lens).

We start with a photon at a distance  $r$  from the centre  $O$  of a spherically symmetric lens of mass  $M$  and radius  $R$ . The Schwarzschild radius of the lens is  $R^*=2GM$ . We define  $\lambda$  and  $\rho$  from  $R^*=\lambda R$  and  $r=\rho R$ . We choose the  $x$  axis as the line joining the centre of the lens to the photon. We call  $\theta$  the angle between the light ray and the line joining the photon to the centre of the lens. From the Schwarzschild metric, it is clear that the photon stays in the  $xOy$  plane which contains the initial ray. The velocity of light at a distance  $r$  from the centre of the lens is  $V=1/\gamma^2$  where one  $\gamma$  factor is for time dilatation and one for space contraction. From Schwarzschild metric  $V=1-2GM/r=1-\lambda/\rho$ .

Moving from 1 to 2 ( $\delta$  infinitesimal),  $r$  increases by  $dr=\delta \sin\theta$  and  $V$  by  $dV=-2GM \partial(1/r)\partial r=2GM \delta \sin\theta/r^2$ . When the photon moves by  $ds$  in 1, it moves by  $ds+d(ds)$  in 2 with  $d(ds)=(dV/V)ds$ . Defining  $d\sigma=ds/R$ , the equal phase plane rotates by  $d\omega=d(ds)/\delta=2GM \sin\theta ds/(Vr^2)=\lambda \sin\theta d\sigma/\rho/(\rho-\lambda)$ .

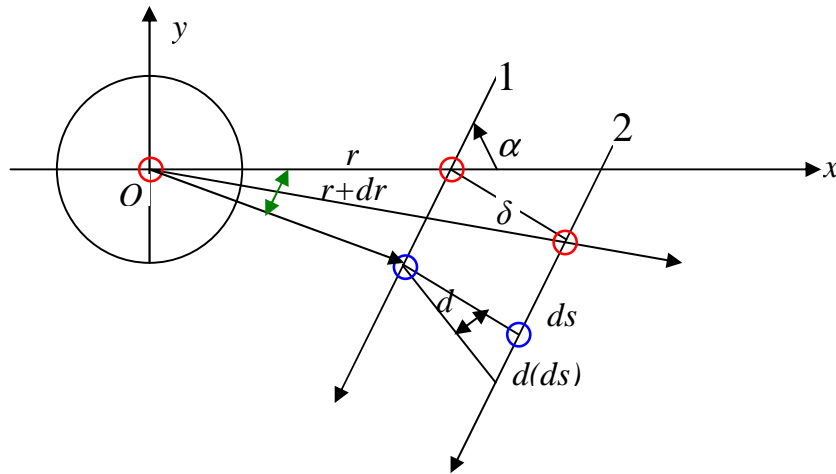


Figure 16. Geometry of light bending (see text).

Moreover, independently from gravitational bending,  $\theta$  changes by  $d\theta = (ds)\sin\theta/r = \sin\theta d\sigma/\rho$ . Therefore, putting both effects together and defining

$$\zeta = \lambda/\rho = R^*/r, \text{ we obtain } d\theta = \sin\theta d\sigma/\rho - \lambda \sin\theta d\sigma/\rho/(\rho - \lambda)$$

$$d\theta/d\sigma = \sin\theta(\rho - 2\lambda)/(\rho[\rho - \lambda]) = (\sin\theta/\rho)([1 - 2\zeta]/[1 - \zeta])$$

This is the equation which we shall be using throughout the present work, using a computer code to trace rays in small steps of  $d\sigma = 0.01$ . Note that  $R$  is absent from this equation: the bending is defined by the ratio between the distance to the lens centre and the Schwarzschild radius of the lens. Of course, when the photon reaches the lens surface it is absorbed and cannot travel farther.

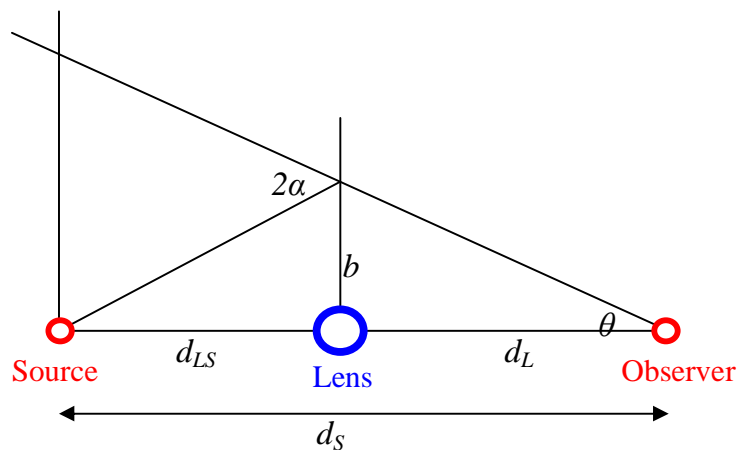


Figure 17. Einstein rings (see text).

Before leaving the subject, let us demonstrate the relation giving the angular aperture of an Einstein ring, which has been mentioned earlier. In the limit of small deviations and perfect alignment (Figure 17),  $\theta d_S = 2\alpha d_{LS} = 4GMd_{LS}/b$  and  $b = \theta d_L \rightarrow \theta^2 d_L d_S = 4GMd_{LS}$  and  $\theta = 2\sqrt{(GMd_{LS}/[d_L d_S])}$ .

### 3.3 Light rays

The fundamental equation of light bending has been computer coded in order to track light rays from a remote source in the vicinity of a gravitational lens. The source has been arbitrarily located 10 lens radii away from the centre of the spherical lens (we say arbitrarily because the source may in fact be chosen anywhere upstream on that ray). As light rays remain in the plane containing the initial ray and the centre of the lens, the problem is 2-dimensional. Rays emitted from the source at various angles  $\alpha_0$  from the line joining the source and the centre of the lens are displayed in Figures 18 and 19 for various values of  $\lambda$ . When  $\alpha_0$  is small, the ray lands on the surface of the lens and is absorbed. When  $\alpha_0$  exceeds some limit angle,  $\alpha_{limit}$ , the ray is bent by the lens and escapes it. For a same value of  $\alpha_0$ , bending increases with  $\lambda$ . The  $\lambda=0$  case (top left panel of Figure 18) corresponds to  $\alpha_{limit} = \arcsin(1/10) = 0.1$ . When  $\lambda$  increases,  $\alpha_{limit}$  also increases and reaches  $\sim 21^\circ$  in the case of a black hole lens ( $\lambda=1$ ). Attempting a precise determination of  $\alpha_{limit}$  reveals a very fast increase of the global bending in its vicinity. This is illustrated in Figure 20 where such light rays are displayed and the dependence of  $\alpha_{limit}$  on  $\lambda$  is shown in Figure 21.

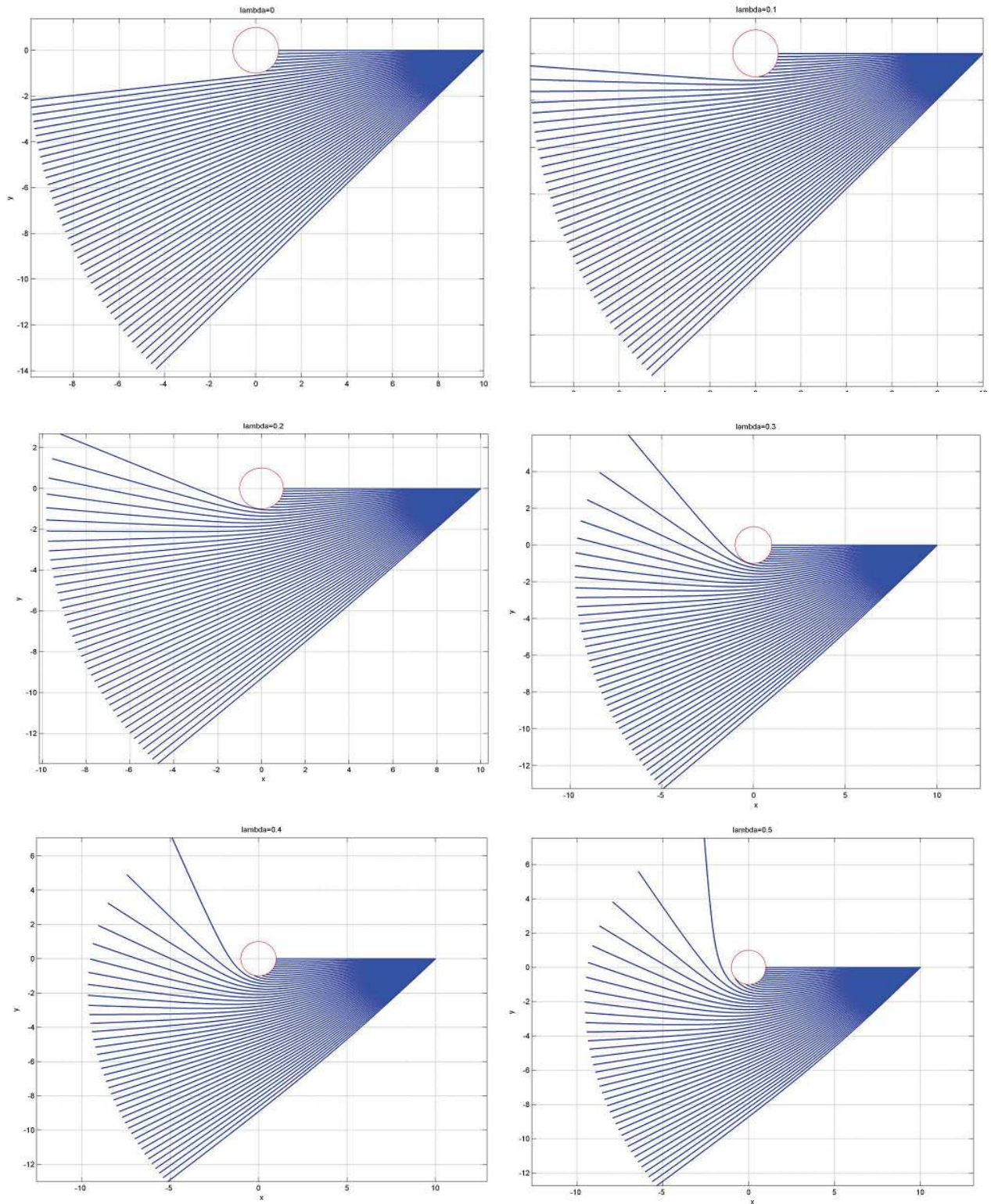


Figure 18. Light rays traced for  $\lambda=0, 0.1, 0.2, 0.3, 0.4$  and  $0.5$ .

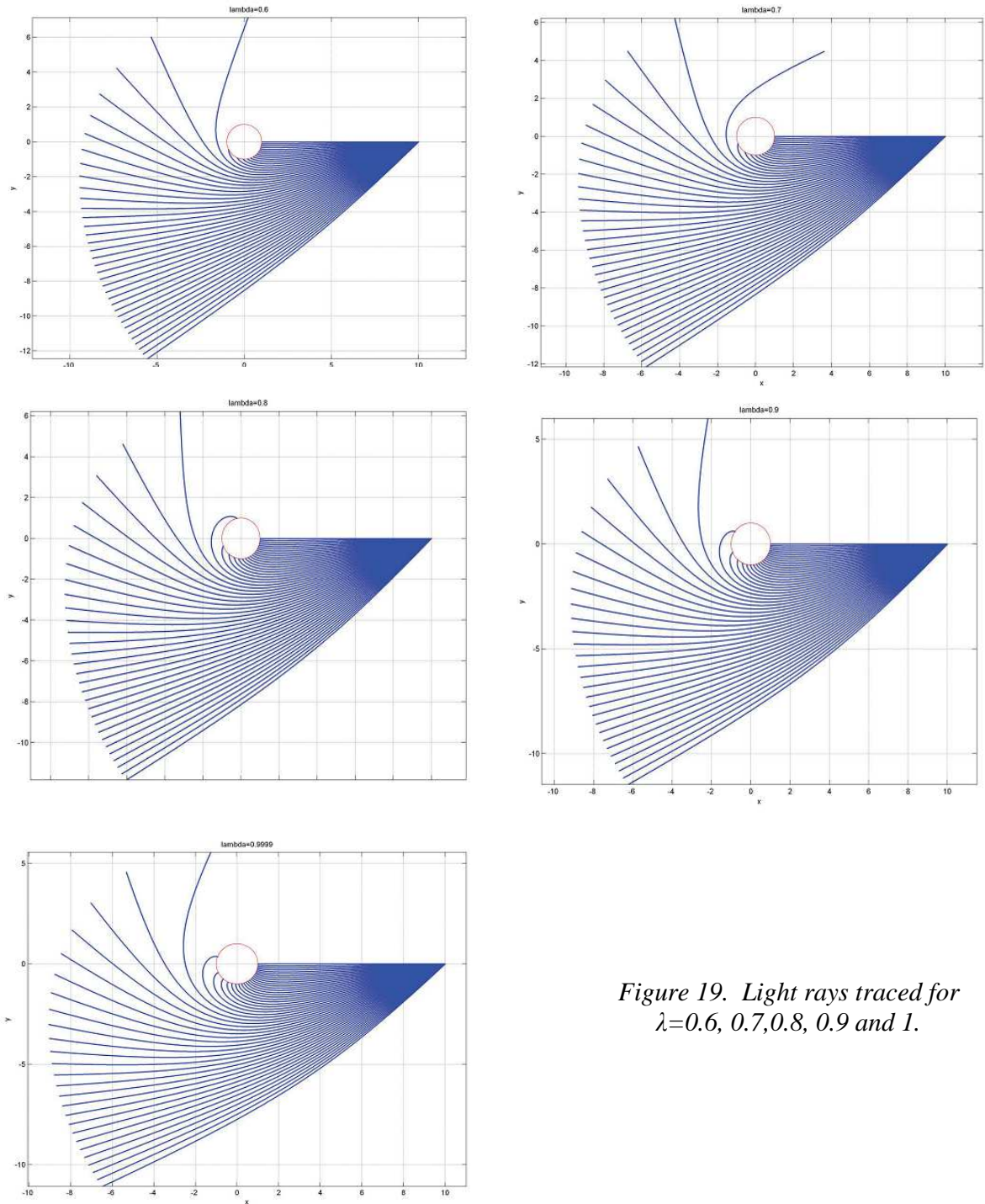


Figure 19. Light rays traced for  $\lambda=0.6, 0.7, 0.8, 0.9$  and  $1$ .

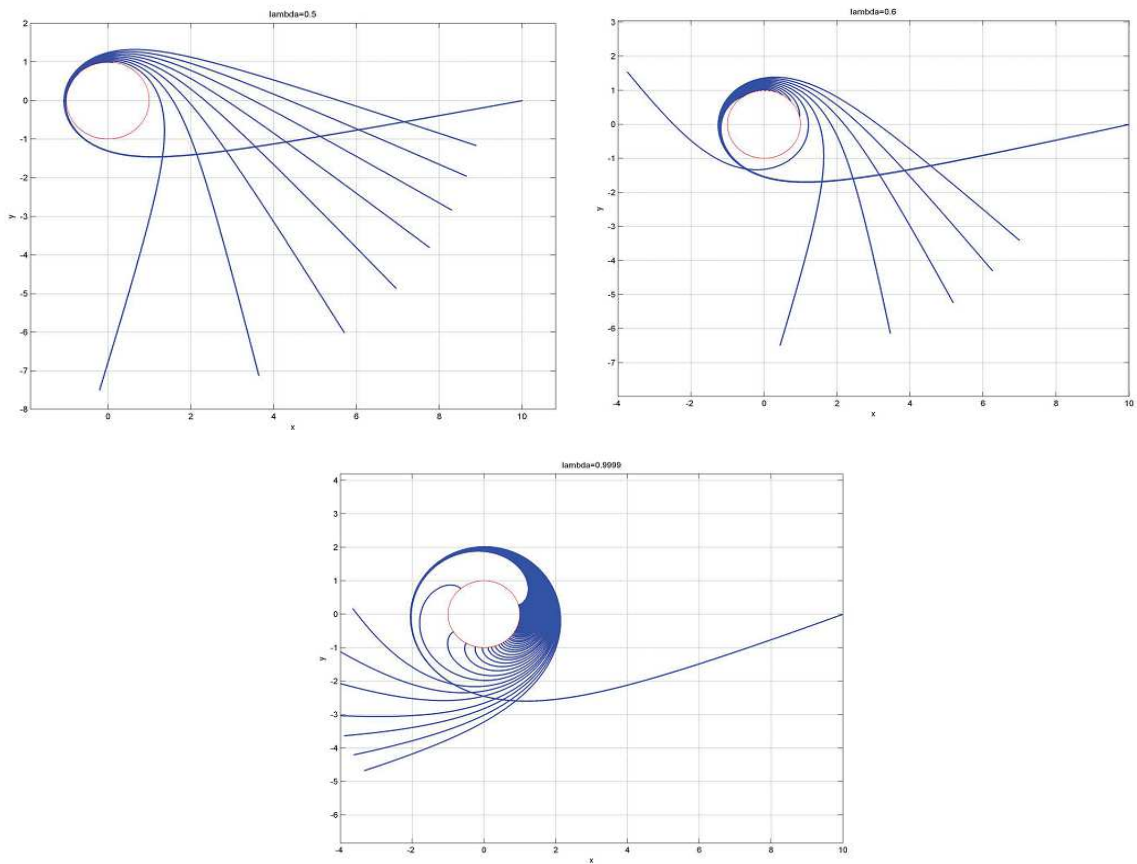


Figure 20. Three examples of rays in the vicinity of  $\alpha_0 = \alpha_{limit}$ . The values of  $\lambda$  are 0.5, 0.6 and 1 respectively.

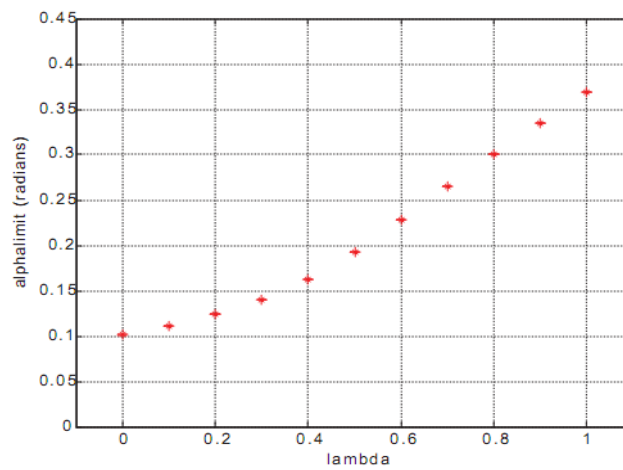


Figure 21. Dependence of  $\alpha_{limit}$  on  $\lambda$ .

We expect rays in the vicinity of  $\alpha_0 = \alpha_{limit}$  to be bent by  $4MG/R = 2\lambda$  as was calculated in Section 3.2 in the small bending approximation. This is indeed what we find with the simulation (Figure 22) but as soon as  $\lambda$  exceeds a few percent, bending increases much faster than linearly and the light ray may indeed curl around the source when approaching the black hole limit.

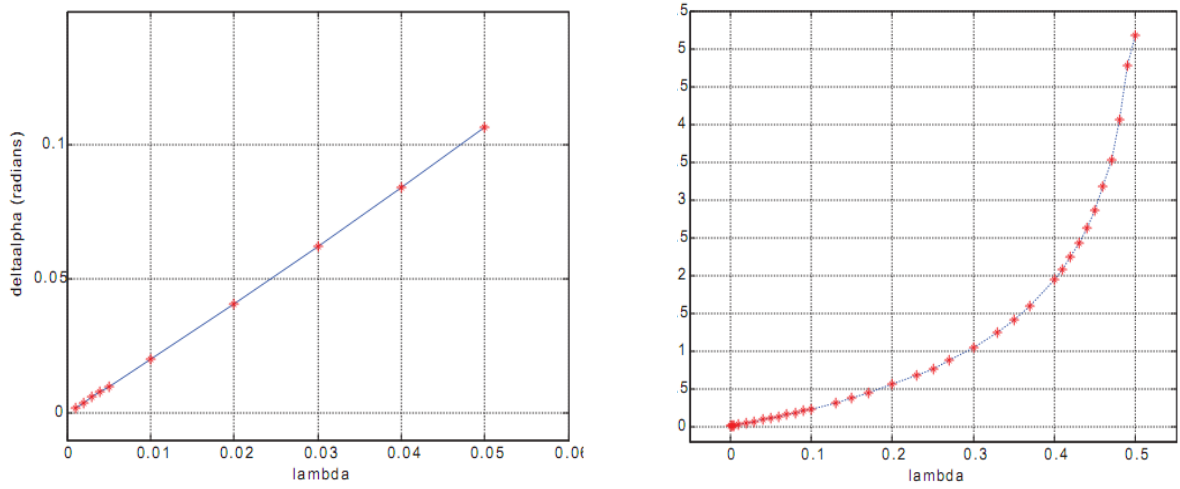


Figure 22. Dependence of  $\Delta\alpha$  on  $\lambda$  for two different ranges of  $\lambda$ .

## 4. Einstein rings

### 4.1 Strategy and useful relations

We now consider the formation of Einstein rings in practical situations, namely for small bending angles at arc minute scale or lower. We restrict the study to spherical lenses. In such cases, the bending angle  $2\alpha$  takes the simple form  $2R^*/b$  where  $b$  is the impact parameter, namely  $\alpha = \lambda/b$ , with  $b$  measured in units of  $R$ , the lens radius. In the plane containing the point source  $S$ , the centre  $L$  of the lens and the observer  $O$ , we have (Figure 23) the angle relations

$$(SAL) = (LAO) = \frac{1}{2}(\pi - 2\alpha)$$

$$(SLA) = \pi - \theta - (SAL) = \pi/2 - \theta + \alpha$$

$$(OLA) = \pi - \theta_E - (LAO) = \pi/2 - \theta_E + \alpha$$

$$(SLA)+(ALO)+(OLP)+\omega=\pi$$

which implies  $2\alpha-\theta-\theta_E+\omega=0$ .

In triangle SAL,  $b/\sin\theta=SL/\sin(\pi/2-\alpha)=SL/\cos\alpha$ .

In triangle OAL,  $b/\sin\theta_E=OL/\sin(\pi/2-\alpha)=OL/\cos\alpha$ .

Defining  $\sigma_S=R/SL$ ,  $\sigma_O=R/OL$ ,  $\sigma_{OS}=\sigma_S+\sigma_O=OS/(SL\cdot OL)$ ,

$b\cos\alpha=\sin\theta/\sigma_S=\sin\theta_E/\sigma_O$  and, to first order in the angles,  $b=\theta/\sigma_S=\theta_E/\sigma_O$ .

Replacing  $\theta_E$  in  $2\alpha-\theta-\theta_E+\omega=0$ , we find  $\theta(1+\sigma_O/\sigma_S)=2\alpha+\omega$

Replacing  $\alpha=\lambda/b=\lambda\sigma_S/\theta$  and defining  $k=(1+\sigma_O/\sigma_S)^{-1}=\sigma_S/\sigma_{OS}$ ,

$\theta=2k\lambda\sigma_S/\theta+k\omega$  giving the second degree equation  $\theta^2-k\omega\theta-2k\lambda\sigma_S=0$ .

Hence,

$$\theta_{\pm}=1/2\{k\omega\pm\sqrt{k^2\omega^2+8k\lambda\sigma_S}\}$$

We define  $\langle\theta\rangle=(\theta_++\theta_-)/2=1/2\omega k$  and  $\Delta\theta=(\theta_+-\theta_-)/2=1/2k\sqrt{\omega^2+8\lambda\sigma_{OS}}$ .

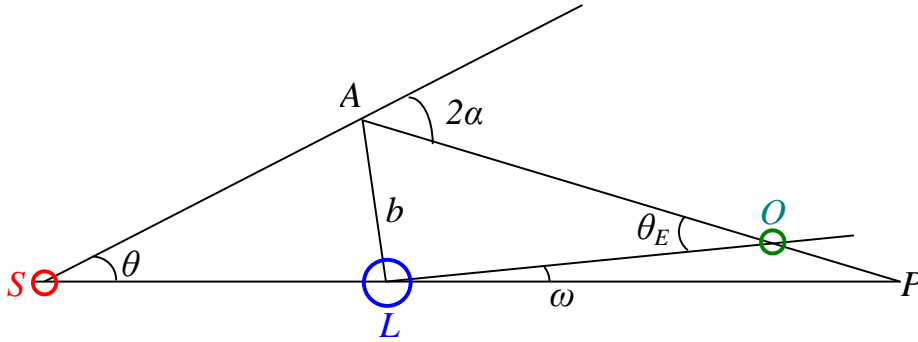


Figure 23. Einstein ring geometry

This equation gives the two rays connecting  $S$  to  $O$  in the  $SOL$  plane. They are on either side of the line  $SL$  and, if one redefines  $\theta=|\theta|>0$ , the two solutions are obviously obtained from each other by simply changing the sign of  $\omega$ .

Consider now a ray emitted by the source out of the  $SOL$  plane, defined by its polar angle  $\theta$  and its azimuth  $\varphi$  around  $SL$ ,  $\varphi$  being measured from the  $SOL$  plane. In

the plane containing the ray and  $SL$  we have, for the impact  $M$  of the outgoing ray on the plane  $O_{\perp}$  containing  $O$  and normal to  $SL$

$$\mathbf{M} = b\mathbf{i} + 1/\sigma_O \mathbf{w} + (\theta - 2\alpha)/\sigma_O \mathbf{i}$$

with  $\mathbf{i} = (\cos\varphi \mathbf{u} + \sin\varphi \mathbf{v})$  and the orthonormal reference frame  $(\mathbf{u}, \mathbf{v}, \mathbf{w})$  defined with  $\mathbf{w}$  along  $SL$  and  $\mathbf{u}$  in the  $SOL$  plane. In this plane, the coordinates of  $O$  are  $\{\omega/\sigma_O, 0, 1/\sigma_O\}$ . The vector  $OM$  has therefore as coordinates in  $O_{\perp}$ :

$$\begin{aligned}\xi &= \{b + (\theta - 2\alpha)/\sigma_O\} \cos\varphi - \omega/\sigma_O = \{\theta/\sigma_S + (\theta - 2\lambda\sigma_S/\theta)/\sigma_O\} \cos\varphi - \omega/\sigma_O \\ \eta &= \{b + (\theta - 2\alpha)/\sigma_O\} \sin\varphi = \{b + (\theta - 2\lambda\sigma_S/\theta)/\sigma_O\} \sin\varphi\end{aligned}$$

which we rewrite as  $\xi = r_M \cos\varphi - \omega/\sigma_O$ ,  $\eta = r_M \sin\varphi$ ,  $r_M = \theta/\sigma_S + (\theta - 2\lambda\sigma_S/\theta)/\sigma_O$

We write  $\theta$  as  $\theta = \langle \theta \rangle + \chi \Delta\theta$  with  $\theta = \theta_{\pm}$  for  $\chi = \pm 1$ . For perfect alignment,  $\omega = 0$ ,  $\theta_{\pm} = \pm\theta_0 = \pm k \sqrt{2\lambda\sigma_{OS}}$ . It is convenient to use  $\theta/k$  rather than  $\theta$  as variable,  $\theta/k = 1/2\omega + 1/2\chi \sqrt{\omega^2 + 8\lambda\sigma_{OS}}$ . Then, as  $k(1/\sigma_S + 1/\sigma_O) = 1/\sigma_O$  and  $\sigma_S/k = \sigma_{OS}$ ,  $r_M = \{(\theta/k) - 2\lambda\sigma_{OS}/(\theta/k)\}/\sigma_O$ .

$$\begin{aligned}\theta/k &= 1/2\omega + 1/2\chi \sqrt{\omega^2 + 8\lambda\sigma_{OS}} \\ r_M &= \{(\theta/k) - 2\lambda\sigma_{OS}/(\theta/k)\}/\sigma_O \\ \xi &= r_M \cos\varphi - \omega/\sigma_O \\ \eta &= r_M \sin\varphi\end{aligned} \quad (4.1)$$

There are two scales for  $\theta/k$ :  $\omega$  and  $\sqrt{(\lambda\sigma_{OS})}$ . It implies also two scales for  $r_M$ :  $\omega/\sigma_{OS}$  and  $\sqrt{(\lambda\sigma_{OS})}$ .

For perfect alignment,  $\theta/k = \chi \sqrt{2\lambda\sigma_{OS}}$  and  $r_M = \{\chi \sqrt{2\lambda\sigma_{OS}} - \sqrt{2\lambda\sigma_{OS}}/\chi\}/\sigma_O = \{\chi - 1/\chi\} \sqrt{2\lambda\sigma_{OS}}/\sigma_O$ , which cancels as expected for  $\chi = \pm 1$  and  $\theta/k = \pm \sqrt{2\lambda\sigma_{OS}}$ , giving

$\theta_E = \theta\sigma_O/\sigma_S = k \sqrt{2\lambda\sigma_{OS}} \sigma_O/\sigma_S = \sqrt{2\lambda\sigma_{OS}} \sigma_O$  and we recover the earlier relation:

$$\theta_E^2 = 2\lambda \sigma_O^2/\sigma_{OS} = 2\lambda(1/d_L^2)/(1/d_L + 1/d_{LS}) = 2\lambda(1/d_L^2)/(d_S/[d_L d_{LS}]) = 2\lambda d_{LS}/(d_L d_S).$$

The solution of Equations 1 depends on the product  $\lambda\sigma_{OS}$  and not on  $\lambda$  and  $\sigma_{OS}$  separately. Lensing a remote quasar by a galaxy ( $\lambda\sim 10^{-6}$ ,  $\sigma_{OS}\sim 10^{-4}$ ) or a nearby star by a foreground stellar black hole ( $\lambda\sim 1$ ,  $\sigma_{OS}\sim 10^{-10}$ ) gives the same ring.

$$\text{For } \chi=0, r_M=(\frac{1}{2}\omega-4\lambda\sigma_{OS}/\omega)/\sigma_O=\frac{1}{2}(\omega^2-8\lambda\sigma_{OS})/(\sigma_O\omega).$$

$$\text{For a source at infinity, } \sigma_S=0, k=0, \theta=0, \theta/k=\frac{1}{2}\omega+\frac{1}{2}\chi\sqrt{\omega^2+8\lambda\sigma_O}$$

$$r_M=(\theta/k)/\sigma_O-2\lambda/(\theta/k).$$

For a lens at equal distances from the source and the observer:

$$\sigma_S=\sigma_O, k=1/2, \theta=\frac{1}{4}\omega+\frac{1}{4}\chi\sqrt{\omega^2+8\lambda\sigma_{OS}}, r_M=2\theta/\sigma-2\lambda\sigma/\theta.$$

For a ray to be seen by the observer, two conditions must be satisfied: it must avoid the lens and it must hit  $O_\perp$  within the angular resolution  $\zeta$  of the detector. The first condition reads  $\theta>\sigma_S$  and the second  $\zeta^2+\eta^2<\zeta^2/\sigma_O^2$ .

We can now draw the appearance of a ring once  $O, L, S, \lambda, \omega$  and  $\zeta$  are given: one simply generates rays emitted from  $S$  at angle  $(\theta, \varphi)$  and checks whether they obey the above conditions. If they do, one plots a point of polar coordinates  $(\theta_E=\theta\sigma_O/\sigma_S, \varphi)$  in the  $(u, v)$  plane. The generation of  $(\theta, \varphi)$  is made with  $\varphi$  uniformly distributed between  $0$  and  $2\pi$  and  $\theta^2$  uniformly distributed in an interval chosen to comfortably bracket  $[\theta_+, \theta_-]$ .

For  $\varphi=0$ , the resolution condition reads  $r_M-\omega/\sigma_O<\zeta/\sigma_O$ , namely  $(\theta/k)-2\lambda\sigma_{OS}/(\theta/k)<\zeta+\omega$ , while for  $\varphi=\pi/2$  it reads  $r_M<\zeta/\sigma_O$ , namely  $(\theta/k)-2\lambda\sigma_{OS}/(\theta/k)<\zeta$ . The latter condition may be rewritten as  $(\theta/k)^2-\zeta(\theta/k)-2\lambda\sigma_{OS}<0$ . The roots are  $(\theta/k)_\pm=\frac{1}{2}\{\zeta\pm\sqrt{\zeta^2+8\lambda\sigma_{OS}}\}$ , and the condition is  $(\theta/k)_-<(\theta/k)<(\theta/k)_+$

$$\zeta-\sqrt{\zeta^2+8\lambda\sigma_{OS}}<\omega+\chi\sqrt{\omega^2+8\lambda\sigma_{OS}}<\zeta+\sqrt{\zeta^2+8\lambda\sigma_{OS}}$$

Setting  $\omega=0$ , we find  $\chi<\{\zeta+\sqrt{\zeta^2+8\lambda\sigma_{OS}}\}/\sqrt{8\lambda\sigma_{OS}}$  and for  $\zeta<<\sqrt{8\lambda\sigma_{OS}}$ ,  $\chi<\zeta/\sqrt{8\lambda\sigma_{OS}}+\sqrt{1+\zeta^2/8\lambda\sigma_{OS}}<1+\zeta/\sqrt{8\lambda\sigma_{OS}}$ .

As in that case  $\theta/k=\chi\sqrt{2\lambda\sigma_{OS}}$ , the relative ring width is  $\frac{1}{2}k\zeta/\theta$ .

Similarly, setting  $\chi=1$ , we find  $\omega+\sqrt{\omega^2+8\lambda\sigma_{OS}}<\zeta+\sqrt{\zeta^2+8\lambda\sigma_{OS}}$ , namely  $\omega<\zeta$ . For  $\varphi=0$ , one has instead  $\omega<\zeta+\omega$ , which is always satisfied. In the  $SOL$  plane, one

keeps seeing images for large values of  $\omega$  while out of the plane the image disappears as soon as the resolution is exceeded.

#### 4.2 Results

We now apply the above considerations to the lensing of a remote quasar by a foreground elliptical galaxy, which we take as spherical. The quasar is taken as pointlike. Assuming a mass of  $10^{12}$  solar masses for the lens, its Schwarzschild radius is  $\sim 3 \cdot 10^{12} \text{ km} = 10^7 \text{ ls} = 3 \cdot 10^{-1} \text{ ly}$ . We take its radius equal to  $3 \cdot 10^3 \text{ ly}$ , meaning  $\lambda = 10^{-4}$ . Taking  $LS = 10^9 \text{ ly}$  and  $OL = 10^8 \text{ ly}$ ,  $\sigma_O = 3 \cdot 10^{-5}$ ,  $\sigma_S = 3 \cdot 10^{-6}$ ,  $\sigma_{OS} = 3.3 \cdot 10^{-5}$  and  $k = 1/11$ . As Equations 4.1 allow for using any common unit for  $\theta$ ,  $\omega$  and  $\lambda$ , we choose to express them in microradians (ppm). We recall that  $1 \text{ arcsec} \sim 5 \text{ ppm}$ . We take  $\zeta = 0.2 \text{ ppm}$ . In ppm, we have therefore  $\sigma_O = 30$ ,  $\sigma_S = 3$ ,  $\zeta = \lambda = 100$ . The result is displayed in Figures 24 to 28 for increasing values of  $\omega$ . The angular coordinates of the ring,  $\theta_E \cos \varphi$  and  $\theta_E \sin \varphi$  are normalized to the size of the ring obtained in the case of perfect alignment,  $\theta_E = \sqrt{(2\lambda/\sigma_{OS})\sigma_O} \sim 75 \text{ ppm} \sim 15 \text{ arcsec}$ . As  $\omega$  increases, the ring quickly splits in two parts. The part on the side opposite to the source fades away and disappears completely for  $\omega = 166 \text{ ppm}$  (last panel of Figure 28) while the part on the source side tends to the non-lensed image of the source.

The focussing properties of gravitational lensing result in an important amplification of the light collected near perfect alignment as illustrated in Figure 29. They are essential in the application to microlensing (Figure 10) and are achromatic: the same curve is obtained when using different filters (Figure 15) and, more generally, radio waves are deflected the same way as visible light, X-rays or  $\gamma$ -rays.

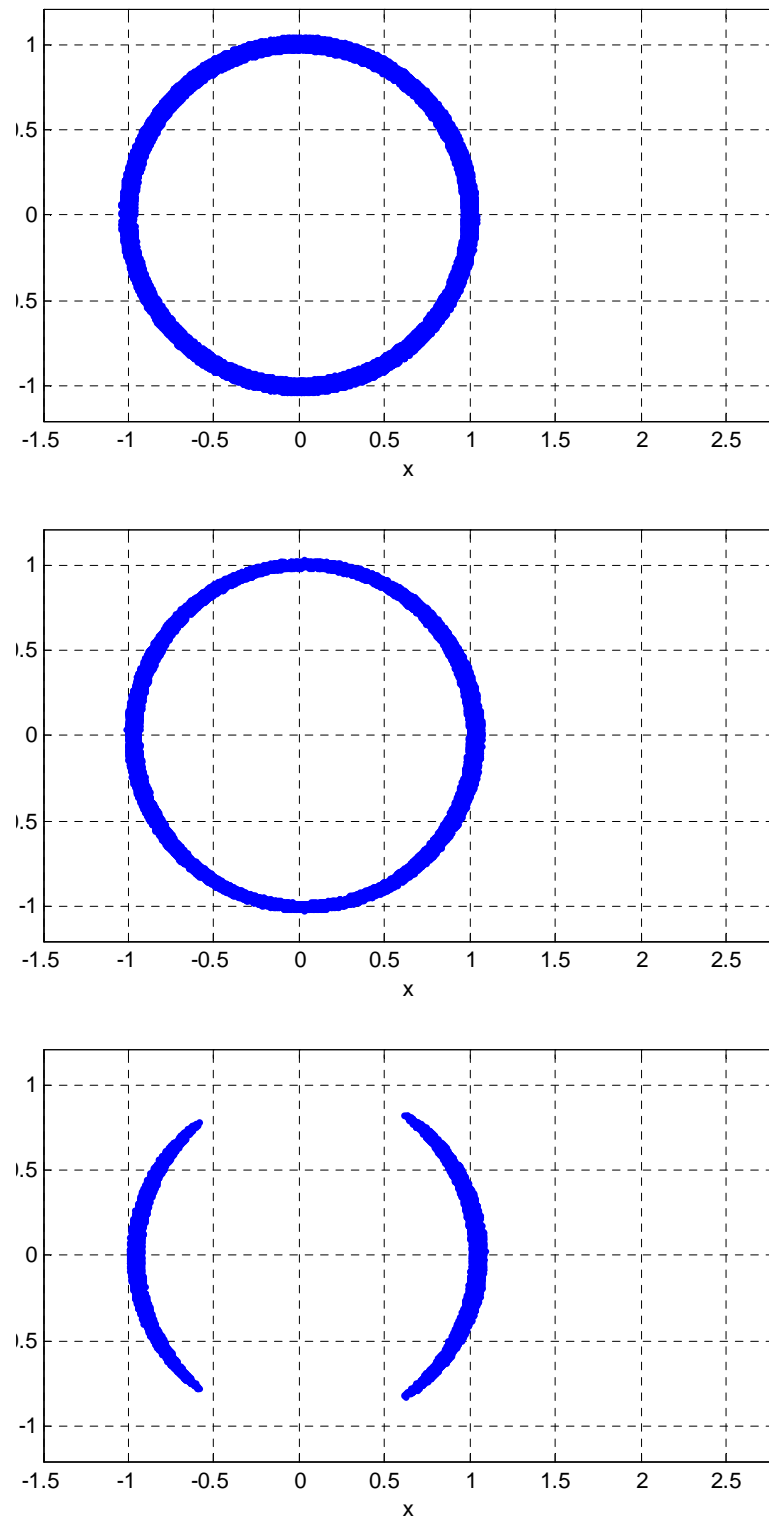


Figure 24. Rings obtained for  $\omega=0, 5$  and  $7.5$  ppm.

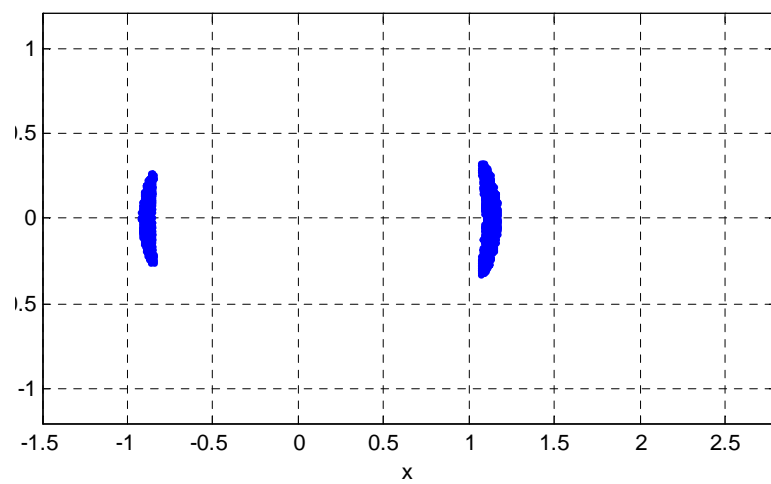
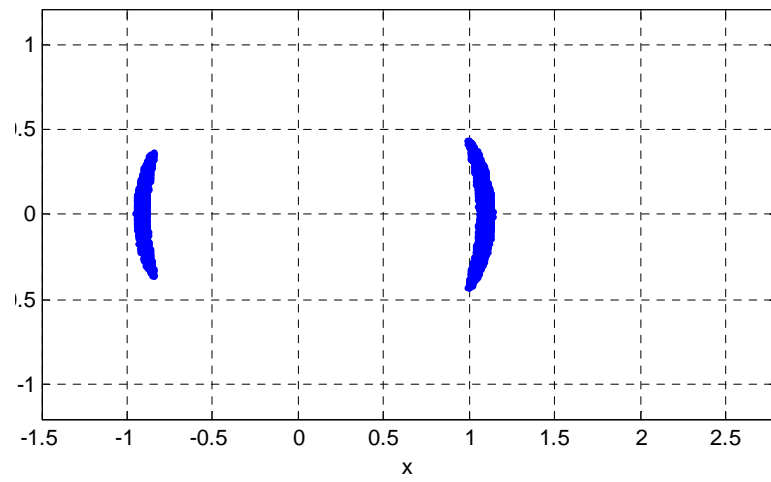
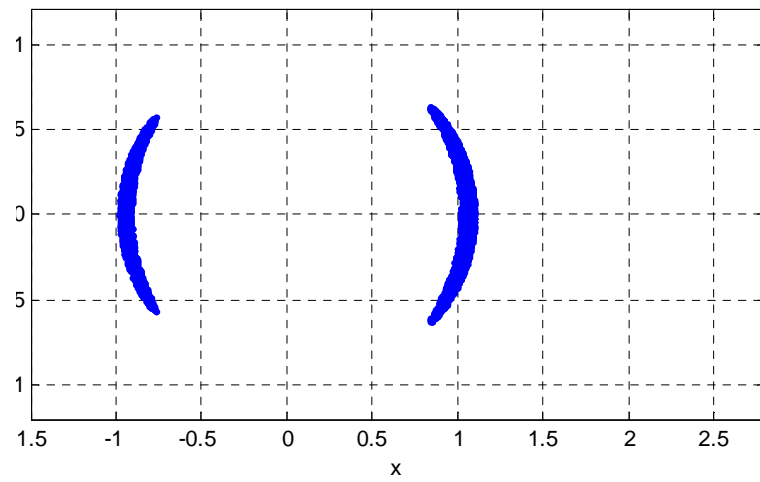


Figure 25. Rings obtained for  $\omega=10, 15$  and  $20$  ppm.

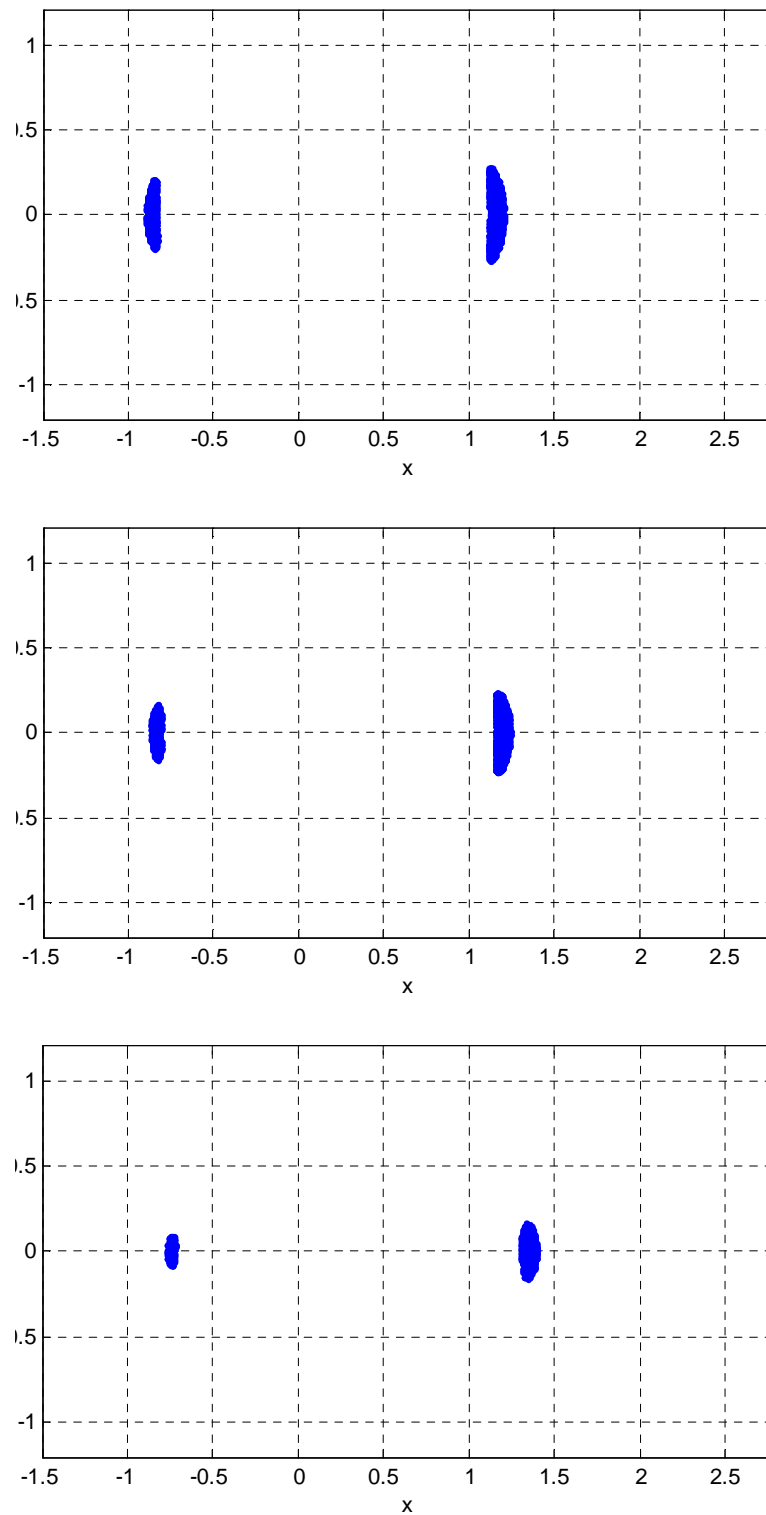


Figure 26. Rings obtained for  $\omega=20, 30$  and  $50$  ppm.

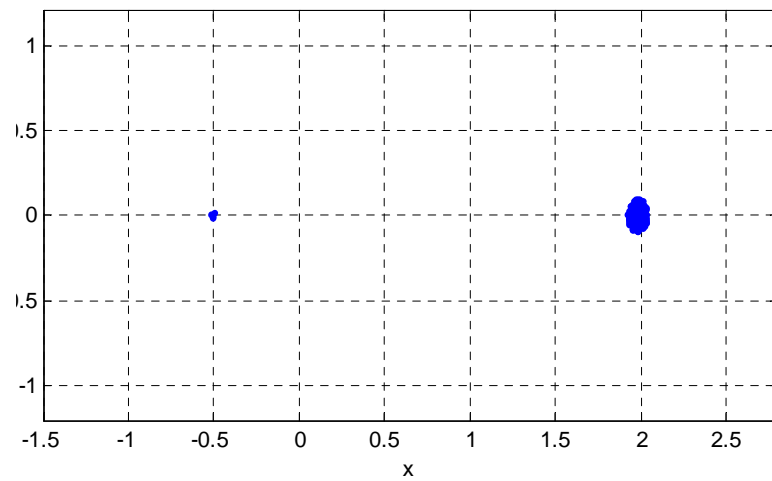
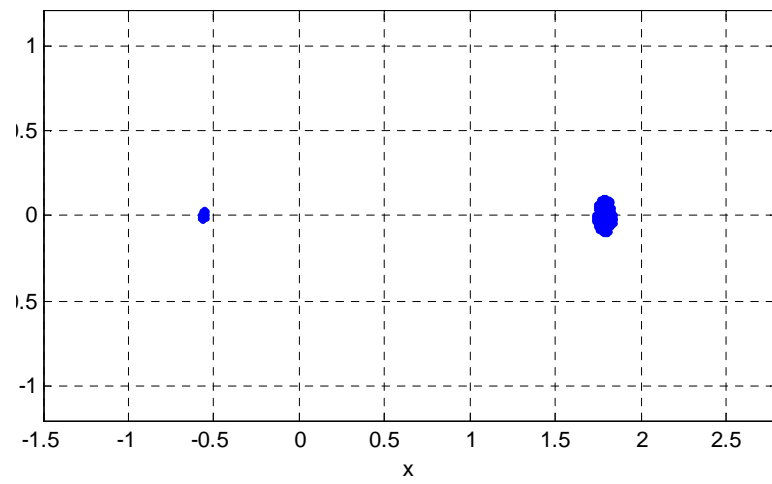
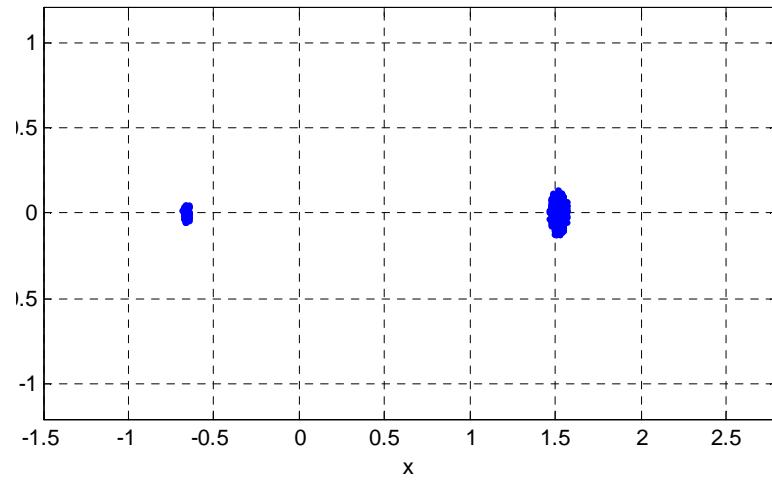


Figure 27. Rings obtained for  $\omega=70, 100$  and  $120$  ppm.

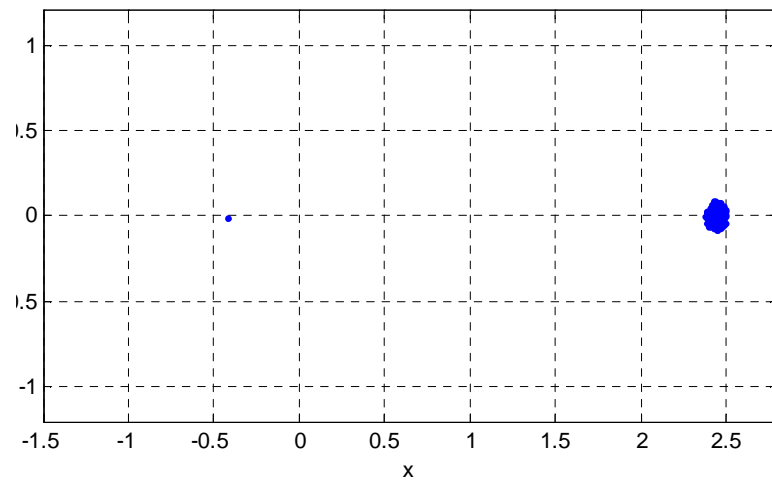
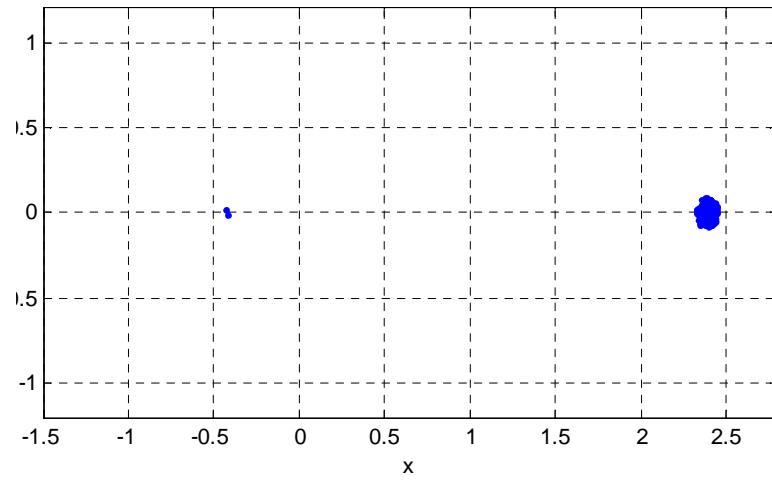
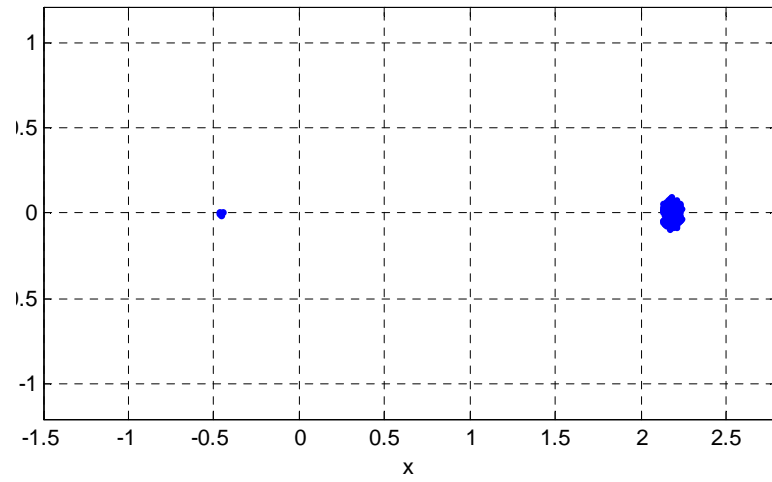
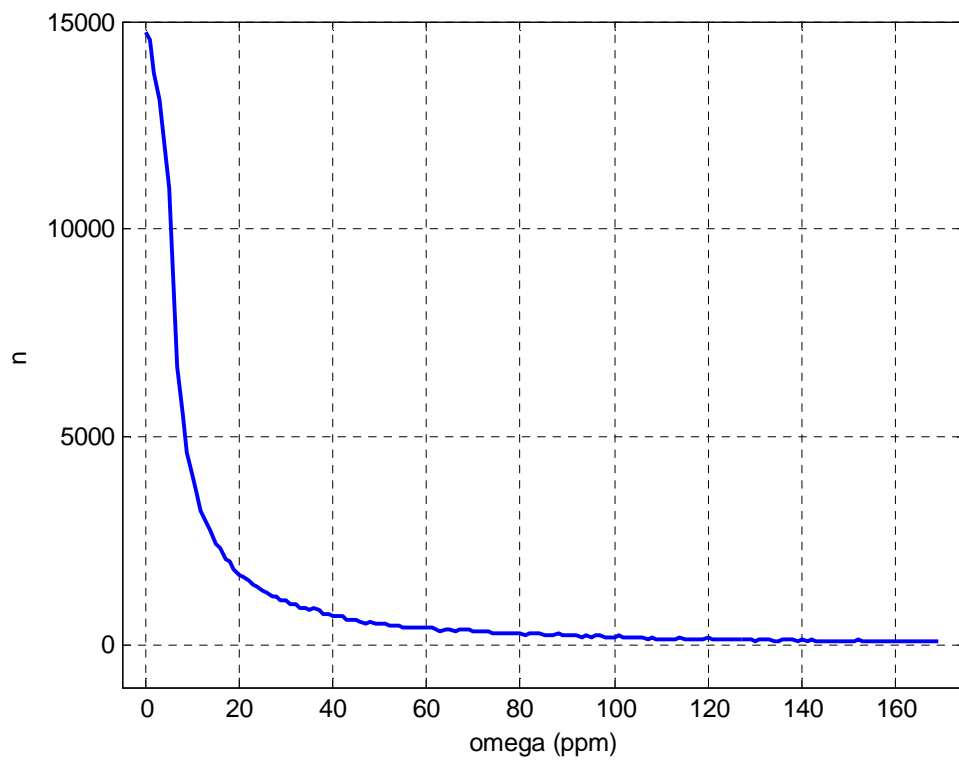


Figure 28. Rings obtained for  $\omega = 140, 160$  and  $165$  ppm.



*Figure 29. Focussing curve showing the dependence of the collected light on  $\omega$ .*

## 5. Conclusion

We have presented a short review of gravitational lensing and the formation of Einstein rings with the aim of describing the main features implied by such phenomena. After a short description of the occurrence of gravitational lensing in astrophysics, including a brief presentation of strong, weak and micro-lensing, the basic underlying physics, special and general relativity, have been introduced. Simulation codes have been written in order to illustrate the behaviour of light in a gravitational field. A first code has made it possible to trace rays in the vicinity of a massive lens, with particular emphasis on the extreme bending that occurs in the vicinity of a black hole. A second code has been used to illustrate the formation of an Einstein ring and its disappearance as the alignment deteriorates. The light amplification that occurs in the case of perfect alignment has been demonstrated.

In practical cases, the non-spherical form of the lens, and to a lesser extent possibly of the source, result in strongly distorted rings, which may take shapes as seen in the Einstein Cross or other similar images. The simulation becomes in such cases much more complicated, each ray must be followed along its path across the complex gravitational field, but this complication is purely technical and of little interest from a physics point of view. For this reason, we restricted the present study to the case of spherical lenses and point like sources, which display the main features of gravitational lensing in a most transparent way.

### ***References***

The introduction and the sections on theory borrow much from the Wikipedia sites on gravitational lensing and references therein as well from P. Darrulat's lectures on "Introduction to cosmology".

- 1) A. Einstein, "*The Foundation of the General Theory of Relativity*", *Annalen der Physik*, 49 (1916) 769.
- 2) F.W. Dyson, A.S. Eddington and C. Davidson "*A determination of the deflection of light by the Sun's gravitational field, from observations made at the total eclipse of 29 May 1919*", *Philos. Trans. Royal Soc. London* 220A (1920) 291.
- 3) O. Chwolson, "*Über eine mögliche Form fiktiver Doppelsterne*", *Astronomische Nachrichten* 221 (1924) 329.
- 4) A. Einstein, "*Lens-like Action of a Star by the Deviation of Light in the Gravitational Field*", *Science* 84 (2188) (1936) 506.
- 5) For a discussion of the early history of gravitational lensing, see J. Renn, T.Sauer and J. Stachel, "*The Origin of Gravitational Lensing: A Postscript to Einstein's 1936 Science paper*", *Science* 275/5297 (1997) 184.